Title
The role of COPII coated vesicles in procollagen-1 trafficking

Author
Gorur, Amita

Publication Date
2016

Peer reviewed|Thesis/dissertation

The role of COPII coated vesicles in procollagen -1 trafficking

By

Amita Gorur

A dissertation submitted in partial satisfaction of the

requirements for the degree of

Doctor of Philosophy

in

Comparative Biochemistry

in the

Graduate Division

of the

University of California, Berkeley

Committee in charge:

Randy W Schekman, Chair
Fenyong Liu
Mina J Bissell
Evangelina Nogales De La Morena

Summer 2016

Abstract

The role of COPII coated vesicles in procollagen-1 trafficking

by

Amita Gorur

Doctor of Philosophy in Comparative Biochemistry

University of California, Berkeley

Professor Randy Schekman, Chair

The coat protein complex II (COPII) achieves cargo sorting and vesicle formation at the endoplasmic reticulum (ER) and aids in protein trafficking by the early secretory pathway. The flexibility of the coat machinery to accommodate diverse size and shaped cargo in order to meet the demands of the cell is not well understood. An example of a large cargo protein is collagen, which is synthesized as 300nm precursor fibrils of procollagen in the endoplasmic reticulum (ER). The molecular mechanism by which large procollagen fibrils are accommodated in canonical COPII vesicles of about 70nm remains unclear. Genetic and biochemical evidence for the role of COPII in collagen trafficking has been established in several studies. Recent collaborative work has shown that mono-ubiquitylation of Sec31 by the ubiquitin ligase complex Cul3-Klhl12 leads to the formation of large COPII vesicles (200-500nm) that drive the secretion of collagen. Amongst the follow-up questions from this study were, whether these enlarged vesicles are *bona fide* transport carriers of procollagen and what might the three-dimensional ultrastructure be. This dissertation work aims to characterize the role of large COPII coated vesicles in intracellular procollagen-1 trafficking. Using a combination of *in vivo* imaging techniques and *in vitro* cell-free reconstitution assays, I present evidence that addresses this question.

Table of Contents

List of Figures

Acknowledgements

First and foremost, I would like to thank my wonderful family: my husband, Sanjay who is my pillar of support; my son, Pratyush, a bundle of positive energy and my constant motivator who is also thrilled to graduate from Elementary School as I graduate with a doctoral degree; my in-laws who are a constant source of encouragement and my loving parents.

I would like to thank past and current members of Schekman and Auer Labs especially Kanika, Pengcheng, David and Purbasha. My special thanks to Lin, a great colleague always ready to help out. Many thanks to Sam at Xu Lab, Prof. Michael Rape, Colleen and Lingyan at Rape Lab for collaborative work.

I would like to thank Dr Manfred Auer at LBL and the employee assistance program that supported me with tuition reimbursement all through my Graduate Studies.

I would like to thank Bob, our wonderful lab manager, who is certainly the most well-organized.

I am indebted to Kent McDonald and Reena at EML who have helped me with tremendous technical support and discussions.

I would like to thank my Thesis Committee members for their advice and guidance.

Thank you Steve and Denise, I have spent countless hours at your fantastic imaging facility.

Thank you Ann and Alison for your excellent Tissue Culture facility.

My remembrance and deep gratitude to Dr. Bill Costerton who passed away in 2012.

No words adequately justify my gratitude and respect for my PhD advisor Prof. Randy Schekman, a mentor with integrity and patience, who continues to teach us by example of who a disciplined, persevering and a modest scholar is irrespective of attaining immense success and knowledge.

I feel truly blessed with many well-wishers and friends who have helped me along the way!

Chapter 1: Introduction of vesicular trafficking

The secretory pathway is responsible for the synthesis, folding, and delivery of a diverse array of cellular proteins. Secretory protein synthesis begins in the endoplasmic reticulum (ER), and once ready for forward traffic, proteins are captured into ER-derived transport vesicles that form through the action of the coat protein complex II (COPII) coat (Barlowe, 1994).

COPII coat assembly

The COPII coat machinery consists of five cytosolic proteins: Sar1, Sec23, Sec24, Sec13 and Sec31. COPII assembly on ER membranes is initiated by the activation (i.e., the GDP–GTP exchange) of the small GTPase Sar1 promoted by the guanine nucleotide exchange factor Sec12, an integral ER membrane glycoprotein. Activated Sar1 initiates vesicle formation by inserting an N-terminal amphipathic helix into the ER membrane, generating membrane curvature, and by recruiting the coat components Sec23/24 (inner layer), establishing the pre-budding complex, and subsequently Sec13/31 (outer layer). Cargo laden COPII-coated vesicles are then delivered to the Golgi via distinct tethering and fusion machineries (Jensen and Schekman, 2011; Barlowe and Miller, 2013).

Transport of large cargo molecules

Since COPII transport carriers have classically been described as spherical vesicles with a diameter of ~60–100 nm, a major challenge in the field is understanding how large/bulky proteins are able to be exported from the ER. In vitro, purified Sec23/24 and Sec13/31 are able to generate empty COPII cages up to 100 nm (Antonny et al., 2003) but these remain too small to accommodate large/bulky cargo proteins that can range from 300 to 1000 nm in diameter. Large lipoprotein particles such as chylomicrons and VLDLs (~80–400 nm in diameter) are secreted from the cell into the bloodstream via specialized vesicles. Fibrillar collagens are synthesized and secreted by fibroblasts as procollagen-I, which folds in the ER into a 330 nm × 1.5 nm elongated rigid rod (Bächinger et al., 1982). Such structures would clearly be too large to be contained by conventional COPII vesicles.

Procollagen secretion is COPII dependent

Several studies suggest that procollagen secretion is COPII-dependent. Procollagen secretion is defective in cells expressing a GTP-hydrolysis-defective Sar1AH79G mutant, as well as in fibroblasts deficient in Sec13–31 (Townley et al., 2008). The membrane accessory protein TANGO1/Mia3 interacts with COPII and is necessary for the export of procollagen VII from the ER in cell culture (Saito et al., 2009). Mia3-knockout mice are neonatally lethal and produce cells defective for secretion of numerous collagens, including collagen I, II, III, IV, VII and IX (Wilson et al., 2011). It

has been proposed that the interaction between TANGO1/Mia3 and Sec23– 24A stalls the formation and subsequent scission of the COPII-coated vesicle until the large procollagen molecule is packaged (Saito et al., 2011; Malhotra and Erlmann, 2011).

Genetic evidence implicating COPII in the transport of procollagen comes from individuals affected with cranio-lenticulo-sutural dysplasia (CLSD). This syndrome is associated with an F382L substitution in Sec23A. Skin fibroblasts cultured from a homozygous patient exhibit a profound delay in collagen secretion; moreover, this mutation inhibits COPII vesicle budding in cell-free assays performed in the presence of Sar1B (Fromme et al., 2007; Boyadjiev et al., 2006). A similar phenotype was described in mice that lack BBF2H7, a transcription factor for Sec23A gene expression (Saito et al., 2009). Likewise, introduction of a premature stop codon in zebrafish Sec23A (crusher) resulted in a malformed craniofacial skeleton (Lang et al., 2006).

Molecular basis for incorporation of large cargo

There is evidence suggesting that the COPII cage is flexible, and it may adapt to coat vesicles carrying large cargoes. For example, a cryomicroscopy study identified strings of interconnected coated buds when yeast COPII proteins were added to giant unilamellar vesicles (Bacia et al., 2010). There is evidence that Sec31 interacts directly with Sar1 to promote Sec23 GAP activity (Bi et al., 2007), and that the affinity of this interaction may differ for the two mammalian Sar1 paralogues. It is proposed that Sar1B might allow for cage expansion (Fromme et al., 2008). The intrinsic flexibility of the Sec13–31 outer cage is also likely to play a major role in vesicle size variation. Two observations contribute to explaining the flexibility of the Sec13–31 coat. First, a number of different architectures could potentially be obtained by rearranging the Sec13-31 subunits into cages with higher geometries (Stagg et al., 2008). Second, comparison of the structure of the yeast Sec13–31 heterotetramer with that of the human Sec13–31 cages has revealed a hinge in the C-terminal Sec31 dimerization interface that may allow protein bending. Using tomography and subtomogram averaging, Zanetti *et al*. describe how coat subunits interact with one another and with the membrane, suggesting how a coordinated assembly of inner and outer coats can mediate and regulate packaging of vesicles ranging from small spheres to large tubular carriers. Recent collaborative work (Jin et al., 2012) has shown that $CUL3^{KLHL12}$ catalyzes the monoubiquitylation of the COPII coat protein SEC31 and thereby drives formation of large COPII carriers. Our current working model is that these large COPII vesicles package procollagen-1 at the ER exit sites and act as transport carriers engaging in anterograde trafficking (Fig 1.1).

About this dissertation

This dissertation aims at understanding the role of COPII coated vesicles in procollagen -1 trafficking. The mechanism of packaging and trafficking regular cargo by canonical COPII vesicles (70-80nm) is well established in the literature, however, it remains to be elucidated whether COPII vesicles play a similar role in packaging large cargo such as procollagen-1. Collaborative work with the Rape Lab established a biochemical mechanism that could render the formation of large COPII coats; however it remained to be confirmed if these vesicles play a direct role in procollagen transport. Chapter 1 tries to answer the question whether the large COPII coated vesicles carry collagen, is collagen completely encapsulated inside a hollow cage, are the vesicles capable of displaying vectorial transport and are collagen-specific chaperones incorporated in the vesicle. The *in vivo* observations are complemented with characterization of the vesicles generated in a cell-free reaction. Chapter 2 aims at understanding the ultrastructure of large COPII coated vesicles. Correlative light and electron microscopy techniques were employed to answer the question whether the large COPII vesicles represent single large vesicles or tubules or clusters of individual vesicles.

Figures

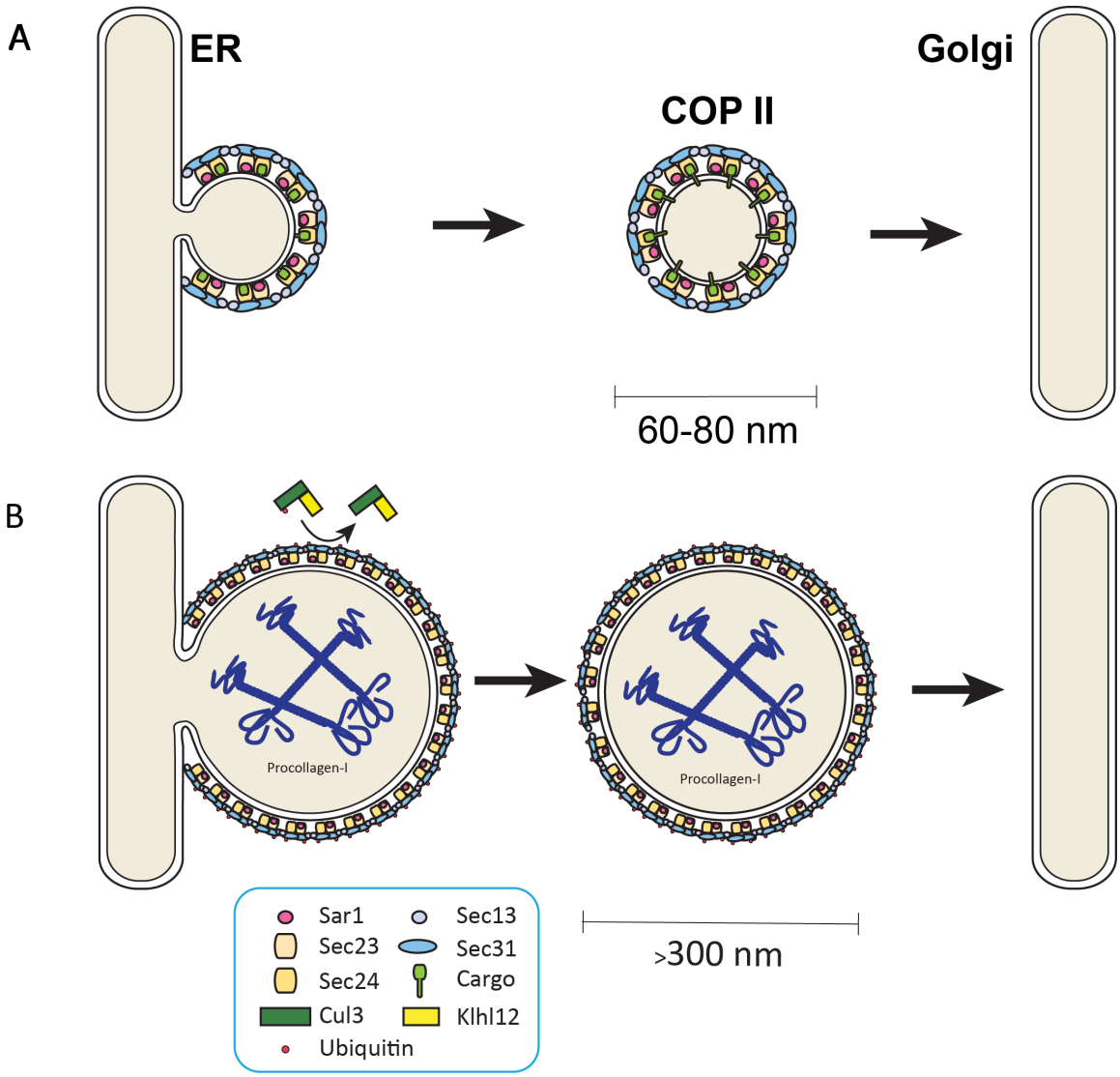

Figure 1.1: Working model of COPII vesicle mediated PC-1 transport

(A) A vast majority of cargo proteins are trafficked by canonical COPII vesicles (60-80 nm) using the COPII coat machinery consisting of five cytosolic proteins: Sar1, Sec23, Sec 24, Sec13 and Sec 31.

(B) Trafficking of large cargo proteins such as procollagen-1 poses a structural challenge on COPII coat machinery. The ubiquitin ligase enzyme, CUL3 engages its substrate adaptor KLHL12 and catalyzes the monoubiquitylation of the outer COPII coat protein SEC31, thereby generating large COPII coated

vesicles. We propose that these large COPII vesicles package and traffic procollagen from the endoplasmic reticulum.

Chapter 2: Elucidating the role of large COPII vesicles as transport carriers of procollagen1 (PC 1)

Introduction

As an essential step in conventional protein secretion, coat protein complex II (COPII) mediates vesicular transport from the endoplasmic reticulum (ER) to the Golgi apparatus in all eukaryotes. The GTPase Sar1, inner coat proteins Sec23/Sec24, and outer coat proteins Sec13/Sec31 are five cytosolic components of the COPII complex, and they are sufficient to generate COPII coated vesicles from synthetic liposomes (Matsuoka et al., 1998; Kim et al., 2005). COPII vesicles were observed to be about 80 nm in diameter by electron microscopy (EM), which potentially limits the transport of large cargos such as the 300 nm long procollagen I (PC1) rigid rods (Barlowe, 1994; Bächinger et al., 1982; Kim et al., 2005). However, human genetic evidence showed that COPII is required to secrete procollagens (PC). Mutations in genes that code for the human COPII paralogs SEC23A and SEC24D were identified to cause the genetic diseases cranio-lenticulo-sutural dysplasia (CLSD) and osteogenesis imperfecta and their characteristic collagen deposition defects during development (Boyadjiev et al., 2006; Kim et al., 2012 ; Garbes et al., 2015).

Although the requirement for COPII to export the large cargo PC out of the ER is clear, the precise role that COPII plays in this process is still unknown. A conventional model was proposed based on the well-studied COPII function for secreting regular cargos. In this model, COPII concentrates large cargos at ER exit sites (ERES), orchestrates the packaging of large cargos into vesicles and the formation of vesicles with structured coats (Fromme and Schekman, 2005). An alternative model suggests that COPII only functions to concentrate large cargos and other factors required for the ER export at ERES, but large cargos exit the ER in other types of carrier than COPII vesicles (Mironov et al., 2003).

The conventional model is paradoxical unless a cellular mechanism exists to increase the size of COPII coated vesicles. Collaborative work has reported that the E3 ubiquitin ligase, CUL3, and one of its substrate adaptor, KLHL12, regulate the size of COPII coated vesicles and the secretion of collagens I and IV (Jin et al., 2012). Overexpression of Klhl12 induced the formation of large COPII structures that were decorated with Klhl2. Most of these structures were more than 300 nm in diameter and large enough to accommodate the large cargo PC1. In this chapter, I examine these large COPII structures that we previously reported and show that they are *bona fide* membranous carriers of PC1 in cells. Moreover, we reconstitute PC1 exiting the ER

inside of membrane bound carriers in a COPII dependent manner. These carriers are purified and shown to be large COPII coated vesicles.

Results

$Cul3^{klhl12}$ regulates the size of COPII coats

The ubiquitin ligase enzyme, Cul3 along with it substrate adaptor, KLHL12 was shown to monoubiquitinate Sec31 (Jin et al., 2012). To identify a role for monoubiquitination by $Cul3^{Klhl12}$, we induced Klhl12-expression in cells and followed the fate of Sec31 by microscopy. Shortly after induction of Klhl12 the majority of Klhl12 and Sec31 co-localized in small punctae (Fig. 2.1A). Over time, these punctae grew into much larger structures that contained most of Sec31, as well as other COPII-components, such as Sec13 or Sec24C (Fig. 2.1 A, B). Sec31 binding-deficient Klhl12-mutants neither co-localized with Sec31 nor induced formation of large structures (Fig. 2.1 C) and depletion of Sec31 blocked formation of large structures by Klhl12 (Fig 2.1 C). Thus, binding of Klhl12 to Sec31 triggers the formation of large COPII-containing structures. When Klhl12 was expressed with a Cul3-mutant that blocks Sec31-ubiquitination ($Cul3^{1-250}$), COPII-structures were not enlarged (Fig. 2.1 C). In addition, depletion of Cul3 by siRNAs, which also abolishes Sec31-monoubiquitylation, prevented formation of large COPII-structures by Klhl12. (Fig. 2.1 A). By contrast, if Klhl12 was expressed with lysine-free ubiquitin to allow mono-, but not multiubiquitylation, large COPII-structures were readily detected (Fig 2.1 C). Immunogold-labeling EM showed comparable structures of 200-500nm that were decorated with Klhl12 (Fig. 2.1 D). Thus, monoubiquitylation by Cul^{Klhl12} promotes formation of large COPII-structures, which likely represent a mixture of nascent coats at ER-exit sites and budded coats on large COPII-vesicles or tubules.

$Cul3^{Klhl12}$ is required for collagen export

Initial screen had linked the role of $Cul3^{Klhl12}$ to the establishment of the stem cell ECM, which is dependent on collagen secretion. Thus, the Cul3-Klhl12 dependent increase in COPII size might function to promote collagen export from the endoplasmic reticulum. To test this hypothesis, we expressed Klhl12 in IMR90 cells, which produce large amounts of collagen, yet accumulate it in the ER due to inefficient export. Strikingly, Klhl12, but not the Sec31-binding deficient $Klhl12^{FG289/290AA}$ or unrelated BTB-proteins, triggered depletion of procollagen I from intracellular ER-pools (Fig. 2.2 A). When secretion was inhibited with brefeldin A, or if procollagen folding in the ER was impaired by removal of ascorbate from the medium, procollagen remained within Klhl12-expressing cells (Fig. 2.2 A). Time-resolved experiments showed that Klhl12 strongly accelerated collagen export from IMR90 cells (Fig. 2.2 B).

Large COPII vesicles co-localize with PC1

To further test whether the large COPII vesicles carry collagen, I used human fibrosarcoma cells (a type IV collagen secreting cell line) stably transfected with proalpha procollagen-1 (KI6) for analyzing puncta (0.2-1μm) generated at 7.5 h of doxycycline induction of expression of Klhl12 . We refer to large COPII vesicles as structures being greater than 200 nm in x-y dimension and positively labeling for a COPII marker and Klhl12. KI6 cells were checked for procollagen-1 expression and secretion based on ascorbate chase assay wherein, after 30 min of ascorbate addition, PC1 was completely secreted out of the cell (Fig. 2.S1A, B).

While using a polyclonal antibody (LF-67) that recognizes the alpha-1 carboxy telopeptide, we observed only partial co-localization of procollagen-1 and Klhl12 and could not satisfactorily demonstrate the fact that the large COPII vesicles generated by overexpression of Klhl12 indeed carry collagen. We reasoned that this antibody perhaps failed to recognize the triple-helical folded conformation of procollagen that is packaged into the transport vesicle. With the use of a monoclonal antibody specific for carboxy pro-peptide, we observed clear co-localization between PC1 and Klhl12 in about 78% of the total puncta (Fig. 2.3 A). These puncta also co-localized with Sec31A, the outer coat protein marker of COPII vesicles (Fig. 2.3 B), indicating an association of these markers with the same organelle. I obtained similar success using another monoclonal antibody that recognizes the N-terminal pro-peptide of PC1 (Fig. 2 .S2A). We observed co-localization of PC1 and KLHL12 puncta in another cell line (svIMR-90), which naturally secrete collagen-1 (Fig. 2 S2 B). I next sought to see if the known procollagen chaperone marker HSP47 (Satoh et al., 1996) co-localizes with the large COPII vesicles and confirmed this by triple immunofluorescence labeling of the markers HSP47, Sec31A and Klhl12 (Fig. 2.3 C). I then compared our monoclonal antibody for PC1 that co-localized with the Sec31A marker to the polyclonal antibody used previously in literature (LF-68) in IMR-90 cells expressing endogenous levels of collagen and Sec 31 proteins. As previously shown, we did not observe any overlap of PC1 and Klhl31A markers using the LF-68 antibody (Fig. 2. S2C).

PC1 is completely encapsulated in large COPII coated membranes

I next sought to dissect the precise localization of PC1 with respect to the COPII coat within puncta that showed co-localization of the two markers. To achieve this, I performed dual and triple color 3D STORM imaging on Sec31A/PC1 co-localizing puncta from cells with over-expressed and endogenous levels of Klhl12. We observed complete cages with hollow cavities that were occupied by the cargo, pro-collagen 1 (Fig. 2.4 A) in HTPC-KI6 cells; in other words, collagen was entirely encapsulated within a cage. When cells prepared similarly were imaged by GSD STORM, we observed a similar pattern (Fig 2.S3. Infact, in this case, we did not observe a complete spherical cage and could represent ER exit sites where cargo concentration occurs in a pre-budding complex. This was also evident in Klhl12/SEC 31A/PC1 co-localizing puncta in Saos-2 cells (Fig. 2.4 B). We also did not observe the presence of procollagen cargo in canonical COPII cages ranging in size of 60-90 nm.

PC1 containing large COPII vesicles exhibit movement

The dynamic nature and organization of ER-to-Golgi transport has been visualized previously with the use of fluorescent labeling and time-lapse microscopy (Scales et al., 1997; Presley et al., 1997; Shima et al., 1999). We sought to understand whether the large COPII vesicles were capable of functioning as mobile transport carriers independent of the ER. We performed double immunofluorescence assays using several ER marker proteins, such as KDEL, calnexin and PDI. While confocal microscopy did not reveal co-localization of large COPII vesicles with ER, we went a step further and confirmed our observation with STORM microscopy (Fig. 2.5 A). We saw clear separation of the organelles with no overlap. The spatio-temporal dynamics of these vesicles became evident when YFP tagged Sec31 labeled structures were observed by time-lapse microscopy in KI6 cells treated with ascorbate for 10 min either in the presence or absence of nocodazole, a microtubule depolymerizing agent. We observed both long range (> 2 um displacement) and short-range transport exhibited by the vesicles in the absence of nocodazole as previously observed for fluorescently tagged COPII vesicles (Stephens et al., 2002) Long range transport was not evident after nocodazole treatment as deciphered by particle tracking of individual vesicles (Fig. 2.5 B, C). Vesicles labeled with YFP-tagged Sec31 and CFP-tagged PC1 also displayed movement (Fig. 2.5 D).

COPII is required to export PC1 out of the ER in a cell-free reaction

To further investigate whether the large cargo PC1 exits the ER inside of COPII-coated vesicles, COPII vesicle formation was reconstituted in a cell-free reaction (Barlowe, 1994; Kim et al., 2005). Donor ER membrane was prepared from the human fibroblasts IMR-90 and incubated at 30°C with purified recombinant human COPII proteins, cytosol, and nucleotides for 1 h to allow the formation of COPII-coated vesicles. The procedure of isolating budded vesicles was modified from our previous reports to allow the detection of large vesicular carriers of PC1. A lower centrifugal speed of 7000 xg was used to sediment donor membrane after a reaction was complete, and the supernatant fraction, which contained budded vesicles, was applied to the bottom of a step flotation gradient. After a high-speed centrifugation step, the top 10 fractions were collected and their contents were analyzed by immunoblotting (Fig. 2.6 A). Because lipid vesicles are more buoyant, they float to the top of the gradient shown by the presence of two model COPII cargos ERGIC53 and Sec22B in the top fraction. Both PC1 and the procollagen-specific chaperone HSP47 floated to the top of the gradient and co-fractionated with ERGIC53 and Sec22B. PC1 and HSP47 in the float fraction were well separated from the PC1 and HSP47 that was present in the supplemented cytosol, which remained at the bottom of the gradient. When the Sar1B H79G mutant was used in place of wild type Sar1B to block COPII vesicle formation, significantly less PC1 remained at the bottom of the gradient. When the Sar1B H79G mutant was used in place of wild type Sar1B to block COPII vesicle formation, significantly less PC1 and HSP47 were detected in the float fraction. This indicates that PC1 was reconstituted to exit ER in association of lipid membranes in a COPII dependent manner. To further investigate other factors

required to export PC1 out of the ER, we conducted the cell-free reaction in the absence of donor membrane, cytosol, and purified recombinant COPII proteins. Immunoblotting of the top float fractions showed that donor membrane, cytosol, purified COPII proteins and the physiological temperature of 30°C were required for the reconstituted export of PC1 (Fig. 2.6 B).

To test whether the PC1 detected in the float fractions was packaged inside of intact vesicles, we employed a collagenase protection assay. When the floated fraction was treated with collagenase, most of the PC1 was protected from the collagenase digestion and only become susceptible when detergent was included to lyse the membrane (Fig. 2.6 C). Together, these experiments showed that the large cargo PC1 is exported out of the ER by packaging inside of intact membrane vesicles in a COPII-dependent manner.

Vesicles generated in the cell-free reaction are COPII coated vesicles containing PC 1

To visualize the membrane vesicles isolated from vesicle formation reaction, we modified this cell-free reaction so that both the large cargo PC1 and the COPII coat were fluorescently labeled. Donor membrane was prepared from cells that were transiently transfected with a GFP tagged construct that labels the C-terminus of pro-α1(I) chain of the human PC1. The COPII coat was labeled by supplementing the reaction with purified Sec23A/24D that was pre-conjugated with Alexa Fluor 647. Vesicles generated from this modified cell-free reaction were visualized by structured illumination microscopy (SIM), and PC1 was found to co-localize with large COPII coated structures approximately 400 nm in diameter (Fig 2.7A). With the resolution of SIM, the PC1-GFP signal was discerned to be within the signal of Sec23A/24D. Smaller COPII structures devoid of PC1-GFP were also observed by SIM and they are likely to be conventional COPII vesicles. Not all large COPII structures observed contain PC1-GFP signal. One possible cause is that only 10% of the donor membrane contained GFP signal due to the low transfection efficiency. Another possibility is that PC1 was not the only large cargo exit the ER in large COPII coated vesicles. Also, not all PC1-GFP observed co-localized with Sec23A/24D, this GFP signal may represent COPII coated vesicles that have undergone uncoating.

Discussion

The function of canonical 80 nm COPII vesicles in conventional cargo transport is well established: The coat concentrates cargo into vesicles exiting the ER while also forming the structural coat of these vesicles (Zanetti et al., 2012). Although a wide range of studies showed that PC secretion is COPII dependent, it has remained unclear whether COPII coats the membranes surrounding the large cargo or instead plays an indirect role in cargo packaging and transport carrier biogenesis. A primary requirement for the transport of large cargos would be to overcome the structural constraints of a small cage. $Cul3^{Klhl12}$ monoubiquitylates Sec31 and promotes formation of large COPII-coats satisfying this requirement (Fig 2.1). Evidence supporting the alternative model that PC is transported out of the ER in non-COPII carriers came from studies of fibroblasts upon

release of a hydroxylation block (Mironov et al., 2003). This study reported that PC1 exit from saccular extensions from the ER that were devoid of the COPII coat based on immuno-fluorescence microscopy and immuno-gold electron microscopy studies using a polyclonal antibody targeting the C-terminal propeptide of the pro-α1(I) chain of PC1. In my study, using two monoclonal antibodies that target the C- or N-terminal propeptides of PC1 respectively, PC1 was observed to co-localize with large COPII structures in unperturbed cells (Fig.2.2B). Moreover, the PC-specific chaperone HSP47 also co-localized with Klhl12 and COPII (Fig. 2.1C). HSP47 preferentially binds to the triple helical form of PC in the ER and accompanies PC to cis-Golgi where it dissociates from PC due to lower pH, after which it is recycled back to the ER by the KDEL receptor (Satoh et al., 1996; Ishida and Nagata, 2011). Hence, this observation confirms that these large COPII structures contained triple helical PC1 and they were physiologically relevant. STORM analyses revealed that collagen becomes completely encapsulated in a large COPII coat during vesicle formation suggesting that COPII proteins participate in PC1 export directly by forming a complete cage around a lipid vesicle that carries PC1 (Fig. 2.2 A, 2B). Furthermore, fluorescently tagged PC1-CFP and COPII outer coat protein SEC31A-YFP also co-localized in live cells, and showed microtubule-dependent vectorial movement (Fig. 2.5 C). In summary, *bona fide* large COPII coated lipid carriers of PC1 were observed in cells.

In an effort to test whether PC1 exit the ER in large COPII coated vesicles, we employed a cell free COPII budding assay (Fig 2.6) that was previously developed in our lab to probe for the budding requirement and efficiency of a number of conventional COPII cargos (Kim et al., 2005; Merte et al., 2010). Using a combination of collagenase protection assay and super resolution fluorescence microscopy, it was seen that PC1 exits the ER inside of large membrane vesicles that are coated with COPII proteins (Fig. 2.6 C, 2.7). This cell-free reaction recapitulates the cellular ER export of PC1 dependence on COPII as little PC1 export was detected when the GTP locked Sar1B H79G mutant was supplemented to the reaction (Fig. 2.6A). Despite being necessary, recombinant COPII proteins alone were not sufficient to reconstitute PC1 budding, as additional cytosol was also required for this process (Fig. 2.6B). This observation is consistent with the literature on the important roles of other cytosolic components, such as cTAGE5, Sedlin, Sly1 and TFG, in exporting PC out of the ER (Saito et al., 2011; Veditti et al., 2012; Noguiera et al., 2014; McCaughey et al., 2016).

In summary, the role of COPII during the ER export of large cargo PC1 was examined using a combination of *in vivo* morphological analyses and *in vitro* reconstitution studies. All of the results obtained support the conventional model where COPII participates directly by forming a large COPII coated membrane vesicle to transport bulky cargo out of the ER. While the exact mechanism by which the size of COPII vesicles is regulated awaits further investigation, the *in vitro* PC1 budding reaction would be a valuable tool for such future studies.

Materials and Methods

Antibodies and plasmids

Commercially available antibodies and dilutions used for immunofluorescence (IF) and immunoblotting (IB) were as follows: rabbit anti-Sec31 A (Bethyl Laboratories, 1:200 for IF and 1:2000 for STORM), mouse anti FLAG (Thermo, 1:5000 for IB) goat anti-FLAG (Novus Biologicals, 1:1000 for IF), chicken anti-KLHL12 (Novus Biologicals, 1:200 for IF, and 1:2000 for STORM), mouse anti-procollagen Type 1 (QED Biosciences, clone # 42024), rabbit anti-calnexin (abcam, 1:200), mouse anti-HSP 47 (Enzo Life Sciences, 1:200 for IF; 1:5000 for IB), sheep anti-TGN 46 (AbD Serotec, 1:200), anti-KDEL (Enzo Life Sciences, 1:200), rabbit anti-GFP (Torrey Pines Biolabs, Inc 1:1000 for IB), rabbit anti ribophorin, ERGIC53, Sec22B were made in house and used at 1:5000 for IB. Rabbit anti-PC1 LF68 and LF41 antibodies was obtained as a gift from Larry Fisher, NIH/NIDCR; LF41 was used at 1:5000 for IB. The mouse anti PC1 antibody SP1.d8 was purified in house from culture media of the mouse hybridoma cells obtained from DSHB at the University of Iowa using standard procedures and used at 3.75 ng/ul for IF. Expression constructs for Sec31A-YFP, Col1A1-CFP and GFP and ER-CFP were kindly provided by David Stephens lab (University of Bristol, UK).

Cell culture and transfection

Human lung fibroblasts IMR-90 and sv-IMR-90, IMR-90 immortalized with SV-40, were obtained from Coriell Cell Repositories at the National Institute on Aging, Coriell Institute for Medical research. Human osteosarcoma Saos-2 and U-2OS, and human fibroscarcoma HT-1080 were obtained from ATCC. IMR-90, sv-IMR-90, Saos-2, U-2OS and HT-1080 were maintained in DMEM plus 10% FBS. The HT-PC1.1 cells line was generated from HT-1080 as previously described in Jin et al., 2012 by stably expressed COL1A1 in a pRMc/CMV plasmid (gift from N. Bulleid) and maintained in 0.4mg/ml G418. The doxycycline-inducible HT-PC1.1 Klhl12-3xFlag stable cell line (HT-PC-KI6) was generated through clonal selection of cells that stably integrated with pcDNA6/TR and Klhl12-3xFlag in a pcDNA5/FRT/TO vector (Flp-In T-REx Core Kit, Thermo Fisher) against 6ug/ml blasticidin and 0.2mg/ml hygromycin, respectively. Cells were kept in a 37°C incubator with 5% CO2. Transfection of DNA constructs into svIMR-90 and HTPC-KI6 cells was performed using lipofectamine 2000 as detailed in the manual provided by Invitrogen. Transfection of DNA constructs to HEK293T cells for cytosol preparation was performed using polyethylenimine (PEI) at the DNA to PEI ratio of 1:3.

Immunofluorescence

Cells growing on poly-lysine coated glass coverslips were fixed in 4% PFA for 30 min, washed five times with PBS and then incubated with permeabilization buffer (PBS containing 0.1% TX-100 and 0.2M Glycine) at RT for 15 min. Cells were then incubated at RT with primary antibody and secondary antibody,respectively. Each antibody incubation was followed by five washes with PBS. Coverslips were mounted in ProLong-Gold antifade mountant with DAPI overnight before imaging. Images were acquired

using Zen 2010 Software on Carl Zeiss LSM 710 confocal microscope system. The objectives used were Plan-Apochromat 100X, 1.4 NA and Plan-Apochromat 100X, 1.4 NA. The excitation lines and laser power used were 488 (4%), 543 (6%) , DAPI (2%) and 633 (6%).

Immunoblotting

Standard immunoblotting procedures were followed. Briefly, samples were heated at 65°C, resolved on 4-20% polyacrylamide gels (15 well Invitrogen; 26 well Bio-Rad), and transferred to PVDF (Millipore). The PVDF membrane was incubated with antibodies and bound antibodies were visualized by an enhanced chemiluminescence method (Thermo) on a ChemiDoc Imaging System (Bio-Rad) with ImageLab software v4.0 (Bio-Rad).

STORM imaging

Dye-labeled cell samples were mounted on glass slides with a standard STORM imaging buffer consisting of 5% (w/v) glucose, 100 mM cysteamine, 0.8 mg/ml glucose oxidase, and 40 μg/ml catalase in 1M Tris-HCL (pH 7.5). Coverslips were sealed using Cytoseal 60. STORM imaging was performed on a home-built setup based on a modified Nikon Eclipse Ti-U inverted fluorescence microscope using a Nikon CFI Plan Apo λ 100x oil immersion objective (NA 1.45). Dye molecules were photo switched to the dark state and imaged using either 647- or 560-nm lasers (MPB Communications); these lasers were passed through an acousto-optic tunable filter and introduced through an optical fiber into the back focal plane of the microscope and onto the sample at intensities of ~2 kW cm^{-2}. A translation stage was used to shift the laser beams towards the edge of the objective so that light reached the sample at incident angles slightly smaller than the critical angle of the glass-water interface. A 405-nm laser was used concurrently with either the 647- or 560-nm lasers to reactivate fluorophores into the emitting state. The power of the 405-nm laser (typical range 0-1 W cm^{-2}) was adjusted during image acquisition so that at any given instant, only a small, optically resolvable fraction of the fluorophores in the sample was in the emitting state. Emission was recorded with an Andor iXon Ultra 897 EM-CCD camera at a framerate of 110 Hz, for a total of ~80,000 frames per image. We performed three-color imaging using two-color channels separately and sequentially using separate emission filters and excitation lasers. A ratiometric detection scheme was employed to concurrently collect the emission of Alexa Fluor 647 and CF680 in the first color channel (Bossi et al., 2008; Testa et al., 2010). Emission of these dyes was split into two light paths using a long pass dichroic mirror (T685lpxr; Chroma), each of which was projected onto one half of an Andor iXon Ultra 897 EM-CCD camera. We performed dye assignment by first localizing and recording the intensity of switching events in each channel. The 560 color channel was subsequently imaged using the reflected light path of the dichroic mirror to minimize misalignment between color channels. For 3D STORM imaging, a cylindrical lens was inserted into the imaging path so that images of single molecules were elongated in misalignment between color channels. For 3D STORM imaging, a cylindrical lens was inserted into the imaging path so that images of single molecules were elongated in opposite directions for molecules on the proximal and distal sides of the focal plane

(Huang et al., 2008). The raw STORM data was analyzed according to previously described methods (Huang et al., 2008; Rust et al., 2006).

Vesicle budding reaction

Vesicle budding reactions were performed as previously described in Kim et al., 2005 with the following modifications. Donor ER membrane was obtained by permeabilizing IMR-90 cells (95% confluent in 3x10 cms dishes) with 20ug/ml digitonin (5 min on ice) and washed with 0.5M LiCl (2mls) in B88 (20 mM HEPES pH7.2, 250mM sorbitol, 150mM Potassium acetate, 5mM Magnesium acetate). Each 100ul reaction contained ATP regeneration system (1mM ATP, 40mM creatine phosphate, 0.2mg/ml creatine phosphokinase), 3mM GTP, purified human COPII proteins (2ug Sar1, 1ug Sec23A/24D, and 1ug Sec13/31A), cytosol (2ug/ul unless otherwise stated, see "cytosol preparation" for details), and donor ER membrane in B88-0 (20mM HEPES pH7.2, 250mM sorbitol, 150mM Potassium acetate). Vesicles generated in vitro were isolated from the reaction mixture in 2 steps. First, donor membranes were sedimented by centrifuging twice at 7000 xg for 5 min each in a swinging bucket rotor (Eppendorf S-24-11-AT). Then, 87.5ul of the supernatant was mixed with 50ul 60% OptiPrep (Sigma-Aldrich) gently until homogenous at the bottom of a 7 x 20 mm tube (Beckman Coulter) and overlaid with 100 ul 18% and 10 ul 0% OptiPrep in B88. The OptiPrep gradient was centrifuged at 250,000xg for 90min (Beckman TLS-55 with adaptors for 7 x 20mm tubes) with slow acceleration and deceleration, after which 20ul fractions were collected from the top and mixed with sample buffer for immunoblotting analysis. When vesicle budding reaction was analyzed by SIM or flow cytometry, the donor ER membrane was prepared from cells (Saos-2, U-2OS or svIMR-90) transiently transfected with Col1A1-GFP using PEI (Sigma) for 96 h. The reaction was supplemented with fluorescently labeled SEC23A/24D. Fluorescent SEC23A/24D was produced as previously described in Bacia et al., 2011 using Alexa Fluor 647 C2 Maleimide (Thermo Fischer).

Cytosol preparation

HT-1080 or HT-PC1.1 cells were cultured to confluence, washed with PBS and gently scraped in B88 with protease inhibitors (Roche). HEK293T cells were transiently transfected with wild type or mutant Klhl12-3xFlag in a pcDNA5/FRT/TO vector and cells were collected 24 h after transfection by pipetting with PBS after a gentle wash with PBS. The collected cells were permeabilized in 80 ug/ml digitonin in B88 with protease inhibitors (Roche) at 4°C with gentle rocking for 30 min. The cell lysate was collected as supernatant after sedimentation at 300xg for 5 min. Digitonin were removed from the cell lysate by incubating with washed Bio-Beads SM2 (Bio-Rad) at 4°C overnight. Bio-Beads were removed by sedimentation at 300xg for 5 min. The supernatant was further centrifuged at 160,000xg for 30min, and the supernatant was collected and concentrated with Amicon Ultra-3k (EMD Millipore) to 40-80 mg protein/ml for use in vesicle budding reactions.

Protein purification

Human Sar1 proteins were overexpressed in *E. coli* and purified as cleaved GST-fusions, as described for hamster Sar1 purifications in Kim et al., 2005. Human SEC13/31A and Sec23A/24D were purified using immobilized metal affinity chromatography from lysates of baculovirus-infected insect cells, as described previously (Kim et al., 2005).

Collagenase protection assay

Top fractions collected after flotation were pooled and redistributed to each reaction to ensure all samples had the equal amount of starting material. Samples were mixed with or without 0.1 unit/ul collagenase (Sigma) in the presence or absence of 1% Triton X-100 (Sigma) and incubated at 30°C for 10min.

Structured Illumination Microscopy Imaging

Vesicles budded from donor ER that expressed Col1A1-GFP and purified Sec23A/24D that was conjugated with Alexa Fluor 647 was collected from the top of the flotation gradient as described in "Vesicle budding reaction". Budded vesicles were mounted in Prolong Diamond (Invitrogen) under No.1.5H coverslips (Zeiss) and set for at least 5 d before imaging to eliminate drift. Z-stacks of 1-2 um were collected in 3 rotations and 5 phases using the 100x/1.46 objective on Elyra PS.1 super-resolution microscope (Carl Zeiss MicroImaging) with less than 2% laser power and less than 400 msec exposure in all channels. Images were reconstructed and channels were aligned using ZEN Black software (Carl Zeiss MicroImaging). 3D iso-surface rendering of each channel was done using Imaris v8.1 (Bitplane USA). Image acquisition, processing, 3D renderings were done using equipment and software in the CNR Biological Imaging Facility at UC Berkeley.

Analysis of collagen export from cells

IMR-90 human lung fibroblasts grown on 100mm dishes in DMEM/10% FBS were transfected with ^{FLAG}Klhl12, ^{FLAG}Klhl12^{FG289AA}, ^{FLAG}Keap1 and pcDNA5-flag using nucleofection kit R (bought from Lonza) as described in the manufacturer's protocol and plated on 6 well plate with 25mm coverslips. When indicated, co-transfections with 2mg each of ^{FLAG}Klhl12 and dominant-negative Cul3 were performed. Dialyzed 10% FBS media was used for ascorbate-free transfections. Brefeldin A (Sigma) was used at a concentration of 2.5 μg/ml and cells were incubated for 30min. MG132 was used at 20mM for 2h, choloroquine was used at 200mM for 1h. Media was collected the next day and cells on coverslips were fixed with 3% paraformaldehyde for 30min and remaining cells on a plate were used to prepare lysates. Cells on coverslips were permebealized with 0.1% Triton for 15min at room temperature followed by blocking with 1%BSA for 30min Primary antibodies used were polyclonal anti-procollagen (LF-67,diluted 1:1000) and anti-flag (diluted 1:200). Secondary antibodies were Alexa fluor 546 donkey anti-rabbit IgG and Alexa Fluor 488 goat anti-rabbit IgG (diluted 1:200). After staining cells with appropriate primary and secondary antibodies, we fixed coverslips on slides using

mounting reagent containing DAPI. Images were analyzed with a Zeiss LSM 710 confocal microscope and captured with Zen10 software. Merges of images were performed with LSM image Browser. Media collected from 6-well plates was normalized with respect to lysate protein concentration estimated using BCA method. Media and lysates of each reaction were checked by immunoblot analysis. Tubulin was used as a loading control for lysates. Ascorbate chase experiments were done by adding ascorbate (0.25mM ascorbic acid and 1mM asc-2-phosphate) to Klhl12-transfected cells, followed by incubation for 5, 10, 30 and 60min.

Figures:

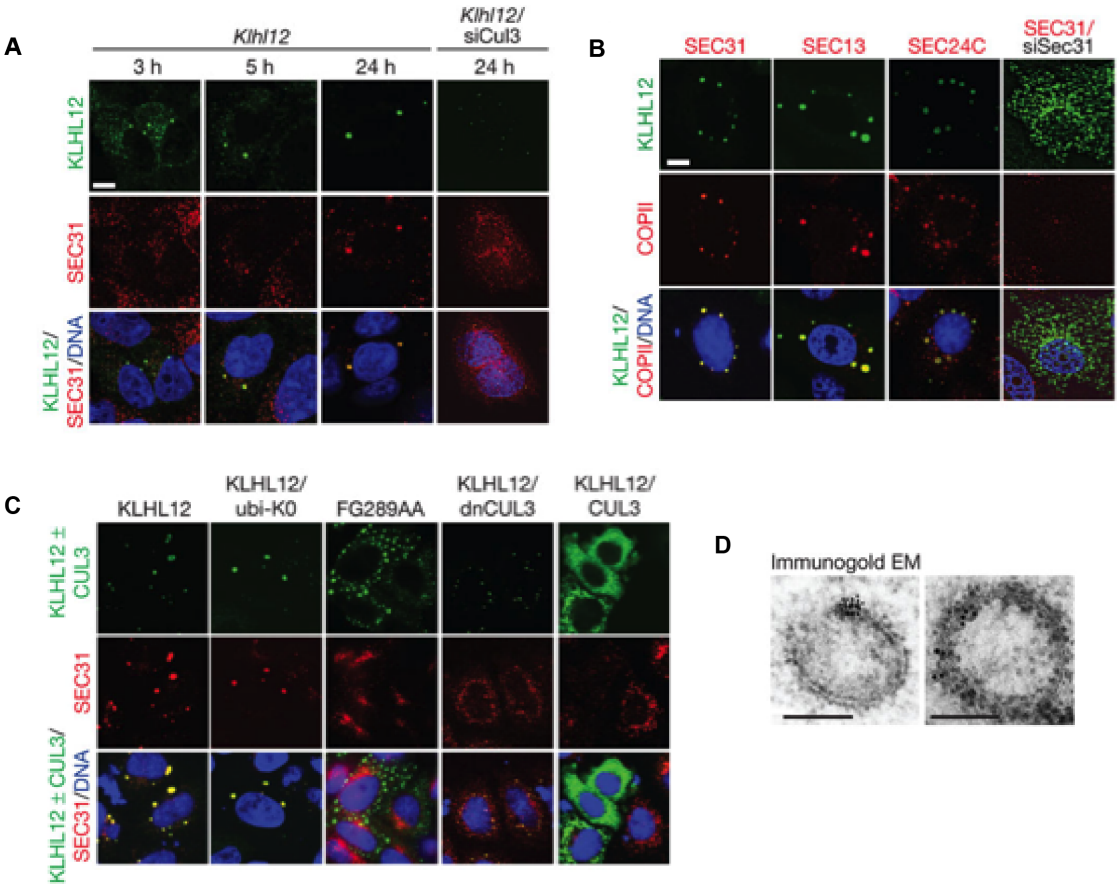

Figure 2.1: Cul3^{Klhl12}-dependent monoubiquitination enlarges COPII-structures. A. Expression of ^{FLAG}Klhl12 was induced in stable 293T cell lines by doxycycline and the localization of Klhl12 (green) and endogenous Sec31 (red) was monitored over time by confocal microscopy. *Right panel*: the experiment was performed in cells treated with siRNA against Cul3. Scale bar: 3μm. **B.** Klhl12-expressing HeLa cells were analyzed for Klhl12 (green) and Sec31, Sec13, or Sec24C (red) by confocal microscopy. Depletion of Sec31 by siRNA (right panel) eliminates formation of Klhl12-dependent structures. Scale bar: 3μm **C.** HeLa cells were transfected with ^{FLAG}Klhl12, lysine-free ubiquitin, ^{FLAG}Klhl12^{FG289AA} (unable to bind Sec31), ^{FLAG}Cul3$^{1-250}$ (unable to catalyze ubiquitination), or ^{FLAG}Cul3, as indicated. Cells were analyzed for abundance and localization of Klhl12/Cul3 (green) and Sec31 (red) by confocal microscopy. Scale bar: 5mm. **D.** Klhl12 localizes to large membrane-bound structures, as detected by immunogold-labeling electron microscopy in HeLa cells transiently expressing Klhl12 (left) or stable 293T cells after Klhl12 induction (right). Scale bar: 200nm.

Note: This figure was first published in Jin et al, 2012.

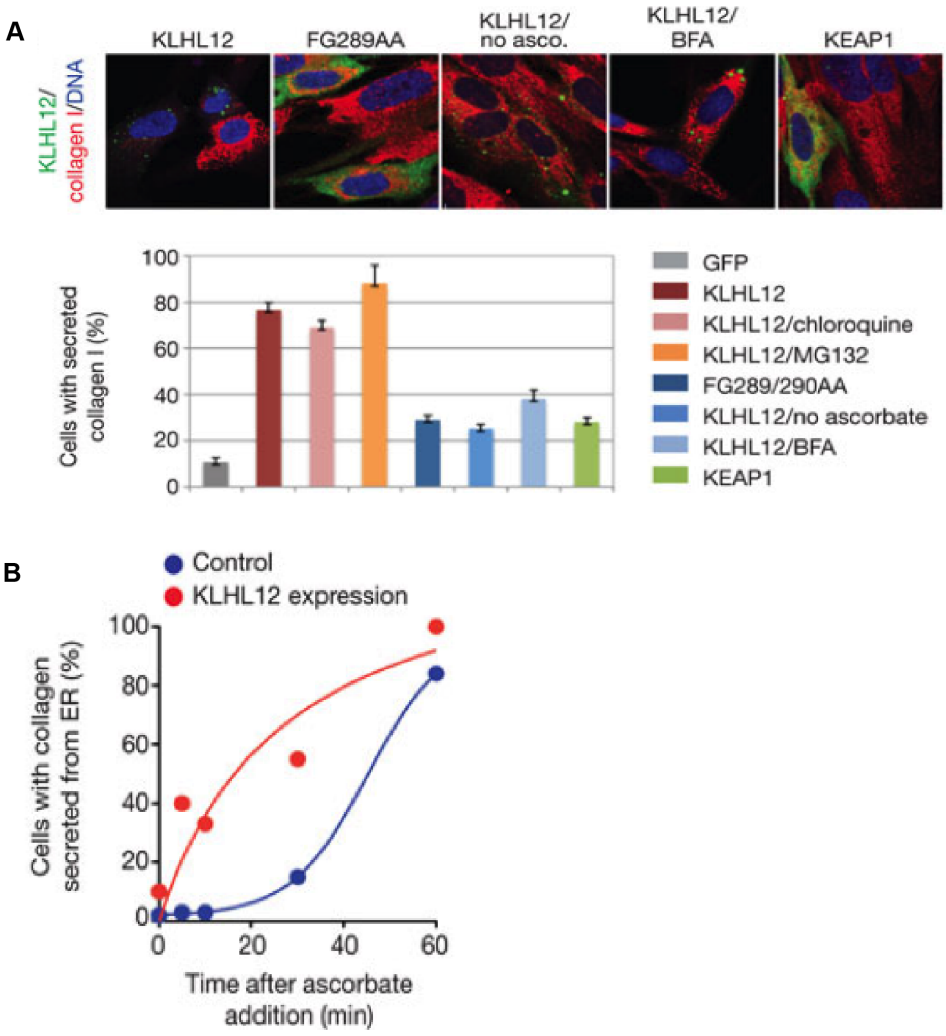

Figure 2.3: Large COPII vesicles co-localize with PC1.

A. KI6 cells were treated with doxycycline for 7.5 h to induce the expression of Klhl12 and immunostained for PC1 (green) and Klhl12 (red). Images shown are average intensity projected views of a Z stack shown for each channel. (i) Colocalizing puncta (indicated by the closed arrow) are displayed as "yellow spots" using the Spot and CoLoc feature in Imaris 8.1.2. Open arrow indicates Klhl12 positive puncta not co-localizing with PC1.

B. KI6 cells immunostained for PC1 (green), Klhl12 (red) and Sec31A (magenta). DAPI is shown in blue.

C. KI6 cells immunostained with HSP47 (green), Klhl12 (red) and Sec31A (magenta). Bars: 10 μm (A); n=3.

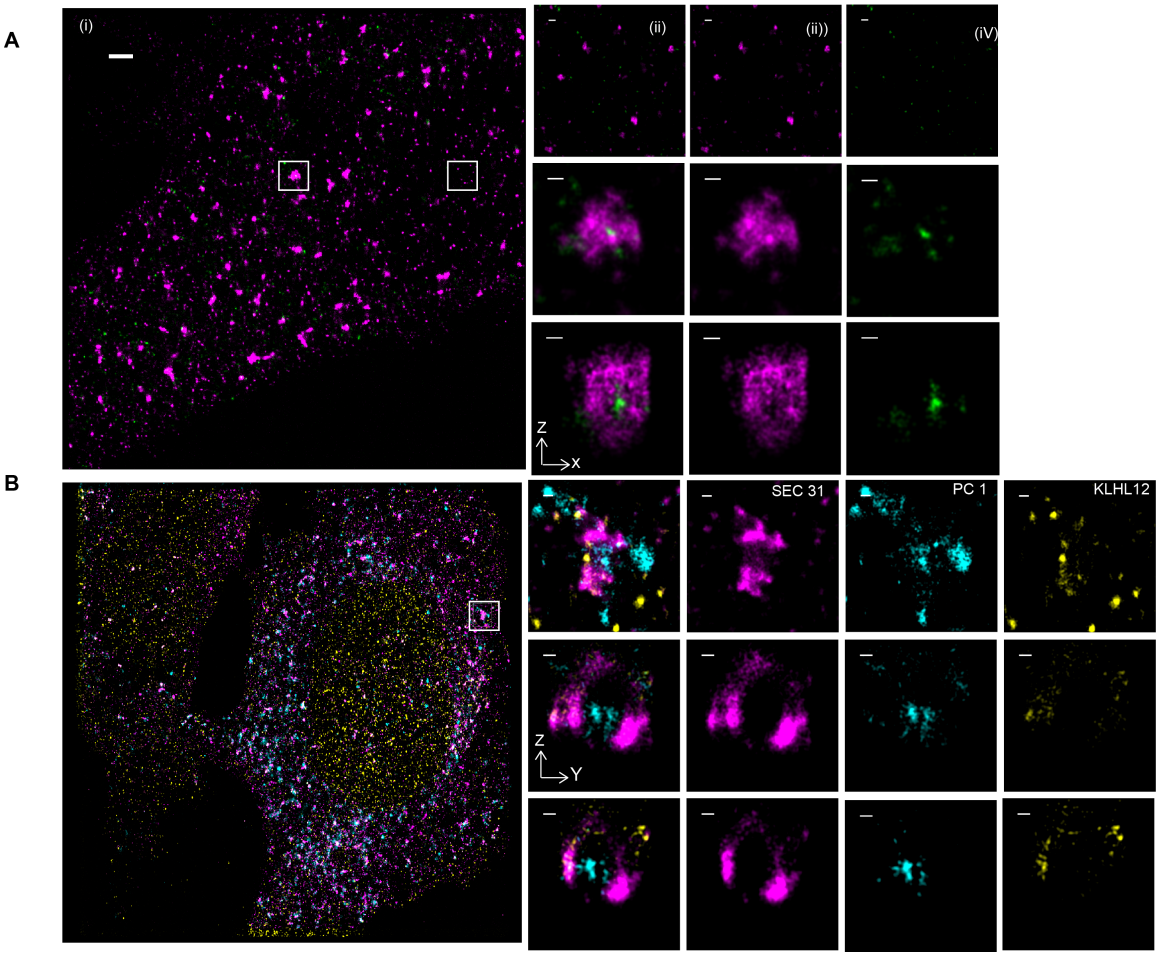

Figure 2.4: Procollagen-1 is completely encapsulated in large COPII coated vesicles
A. KI6 cells were treated with doxycycline for 7.5 h to induce the expression of Klhl12. (i) Two-color 3D STORM of Sec31A (magenta) and PC1 (green) immunostained puncta. Canonical Sec31A puncta (dashed inset; magnified in (ii) as merged image and (iii) Sec31 channel alone; PC1 channel alone in (iv) A virtual XZ section of an enlarged COPII vesicle (solid inset; magnified in iii).
B. SAOS-2 cells were grown at steady state and immunostained for PC1 (teal) , Sec31A (magenta) and Klhl12 (yellow). Triple color 3D STORM imaging with virtual sections in XY, XZ and YZ. Bars: 1 µm (A i, B i); 100 nm (magnified views).

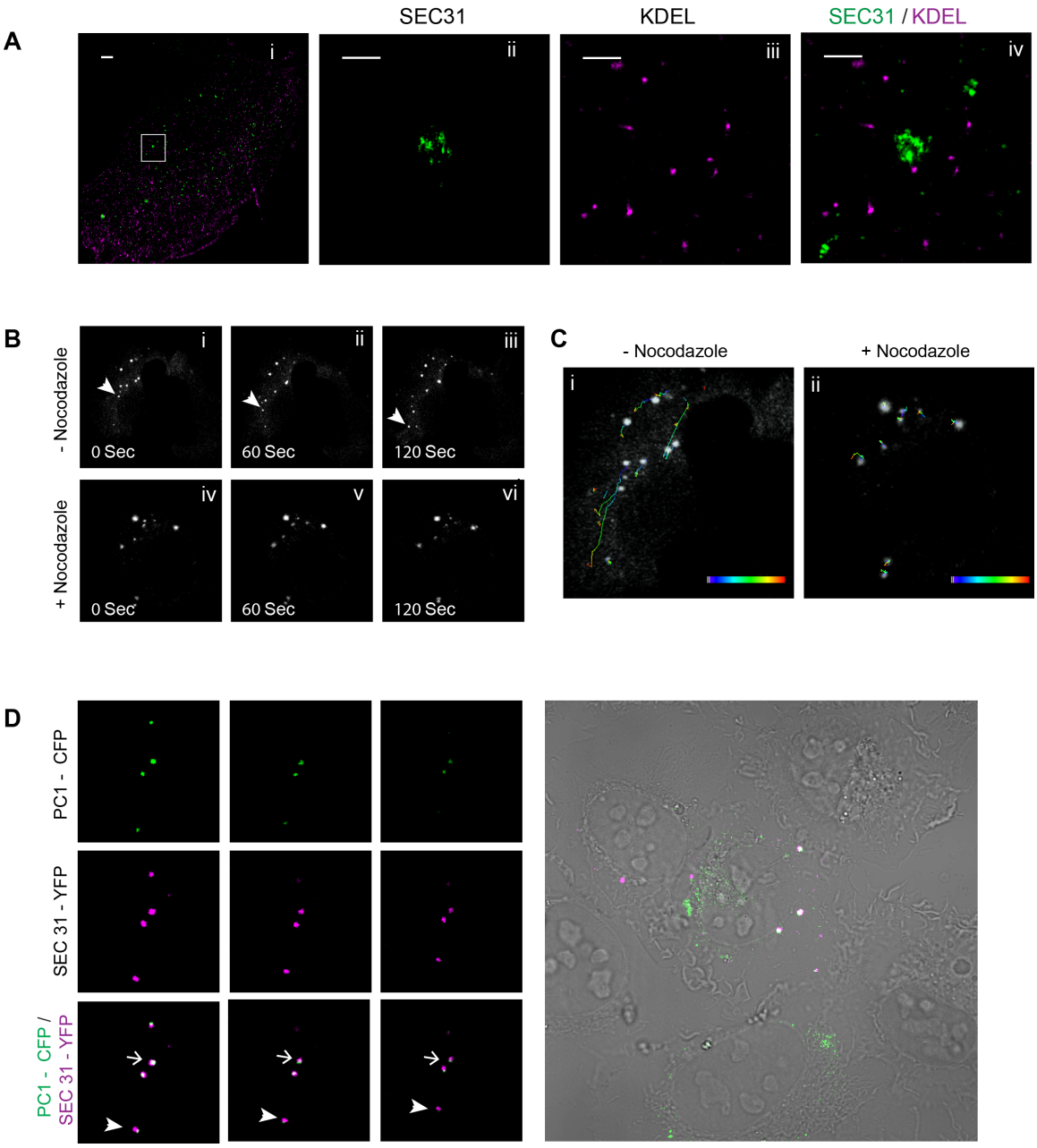

Figure 2.5: Procollagen carrying vesicles exhibit movement.

A. Two color STORM imaging was performed on KI6 cells treated with doxycycline for 7.5 h using KDEL and Sec31A antibodies. (i) Shows a conventional fluorescence microscopy image. Inset in (i) is magnified to show a Sec31A (green)-labeled large COPII cage (ii) KDEL marker labeling ER (magenta) and (iii) shows merged image of the two channels. **B**. KI6 cells were transfected with YFP-tagged Sec31 and induced for Klhl12 expression for 7.5 h. (i-iii) shows time lapse imaging of YFP-Sec31 puncta in the presence of nocodazole. Arrow indicates a puncta exhibiting long-range transport (>10 µm distance). (iv-vi) shows time lapse images of YFP-Sec31 puncta in the presence of 5 µM Nocodazole for 30 min. **C.** Image shown is the first frame of the time-lapse movie

overlayed with the trajectories of YFP-Sec31 puncta in the presence (i) and absence (ii) of nocodazole. **D**. Time lapse imaging of YFP-Sec31 and CFP-PC1 positive puncta in KI6 cells imaged every 5 seconds for a duration of two minutes. Open arrow indicates vesicles appearing to grow smaller in size due to their movement in Z. Closed arrow shows a vesicle that displays a displacement in time.

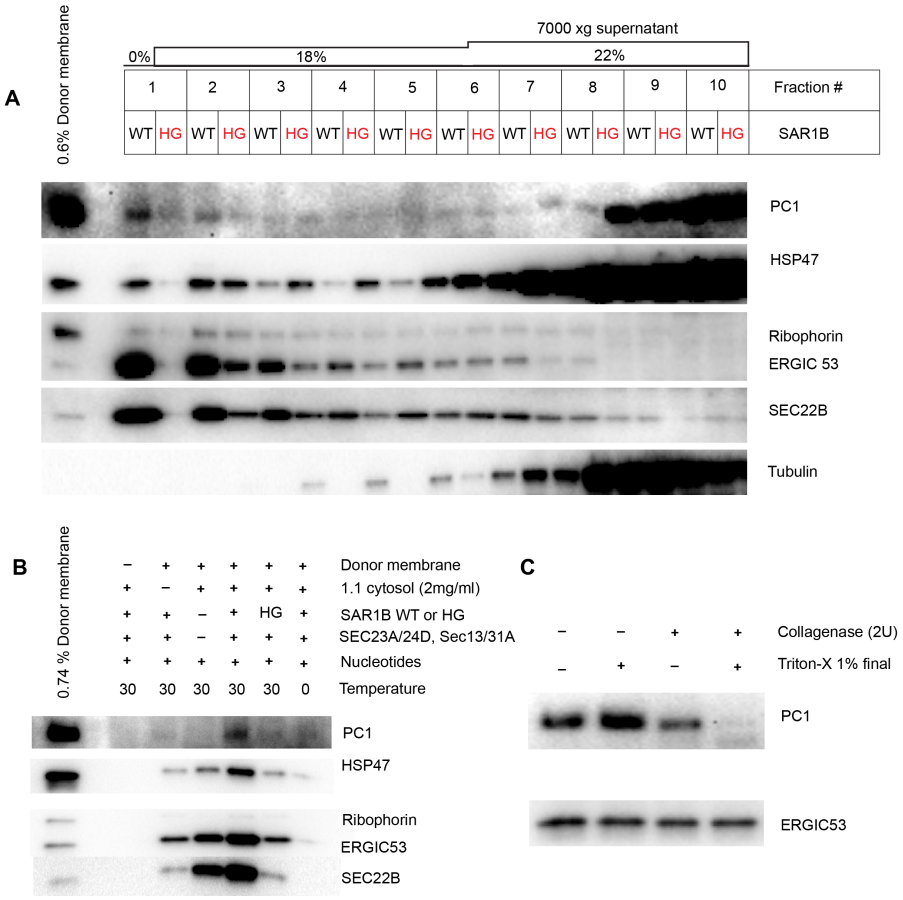

Figure 2.6: COPII is required to export PC1 out of the ER in a cell free reaction. For In vitro vesicle budding reactions see "Materials and methods" for details. Ribophorin I is an ER resident protein that serves as a negative control. ERGIC53 and Sec22B are found in conventional COPII vesicles and serve as positive controls. (A) Vesicles in the 7000xg supernatant fractions from budding reactions that were supplemented with recombinant wild type SAR1B or SAR1B H79G were isolated by flotation. Fractions (10) were taken from the top of each gradient after flotation, and analyzed by immunoblotting. Tubulin was used as a control for soluble proteins that do not float with vesicles. n=2. (B) Budding requirement of PC1 and HSP47 were assessed. Nucleotide represents an ATP regenerating system and GTP. The top fraction after flotation was taken from each sample and analyzed by immunoblotting. n=3. (C) Top float fraction was treated with or

without collagenase in the presence or absence of the detergent Triton X. ERGIC53 was used as loading control. n=2.

A

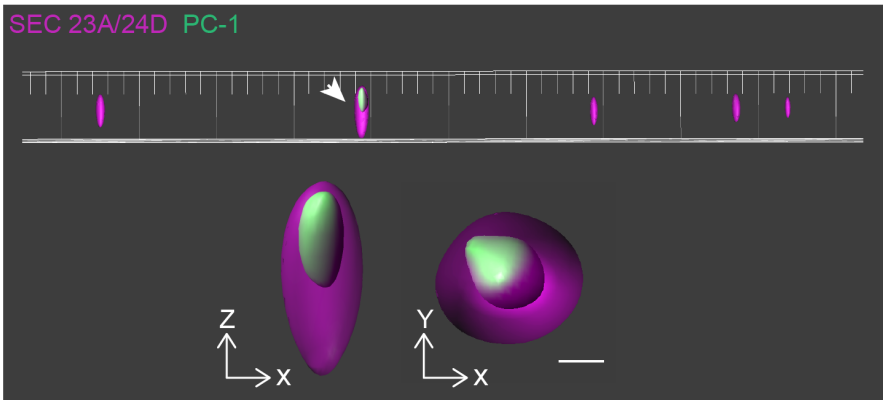

Figure 2.7: Vesicles generated in the cell free reaction are COPIi coated containing PC1

A. Visualization of PC1 carrier isolated from in vitro vesicle budding reaction by SIM, see "Material and methods" for details. A representative field of COPII vesicles, one of them contained PC1-GFP (Green) that was entirely encapsulated by Sec23A/24D-647 (Magenta). Around 20 images were collected from each experiment with no fluorescence and single channel fluorescence controls. n=3.

Supplementary Figures:

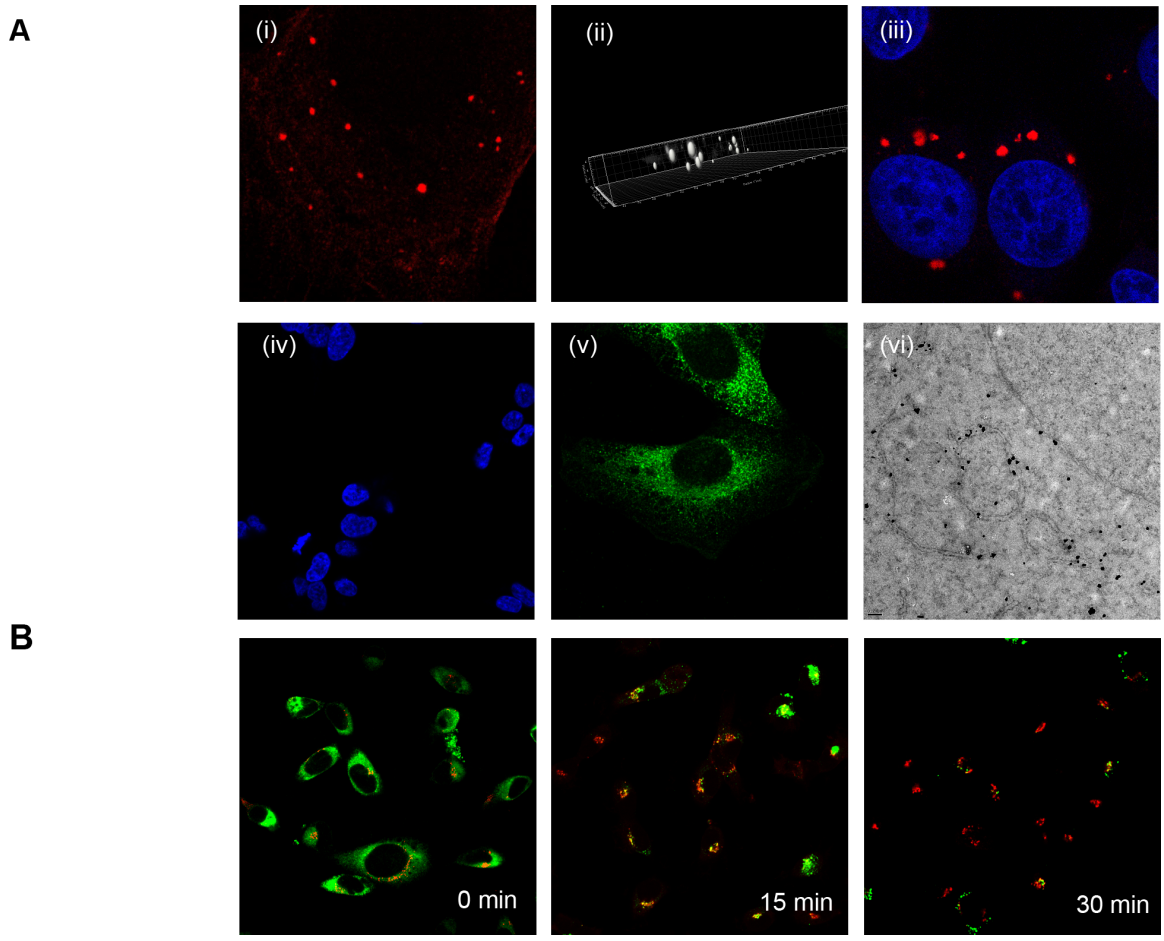

Figure 2. S1. Generation of doxycycline inducible human fibrosarcoma (KI6) cell line stably transfected with PC-1

A. (i) Klhl12 positive structures at 7.5 h of induction with doxycycline. The structures range in z diameter from 0.2 to 1 µm displayed using the spots algorithm in Imaris module (ii) and up to 2µm (x-y) after 24 h induction (iii) Indirect immunofluorescence using PC1 antibody in parent cell line (HTPC 1.1) shows no labeling (iv), while uniform reticular pattern was observed in KI6 cells (v) also confirmed ultrastructurally by pre-embedding immunogold labeling (vi).

B. Ascorbate chase assay performed on KI6 cells shows the movement of collagen at 0, 15 and 30 min after ascorbate addition.

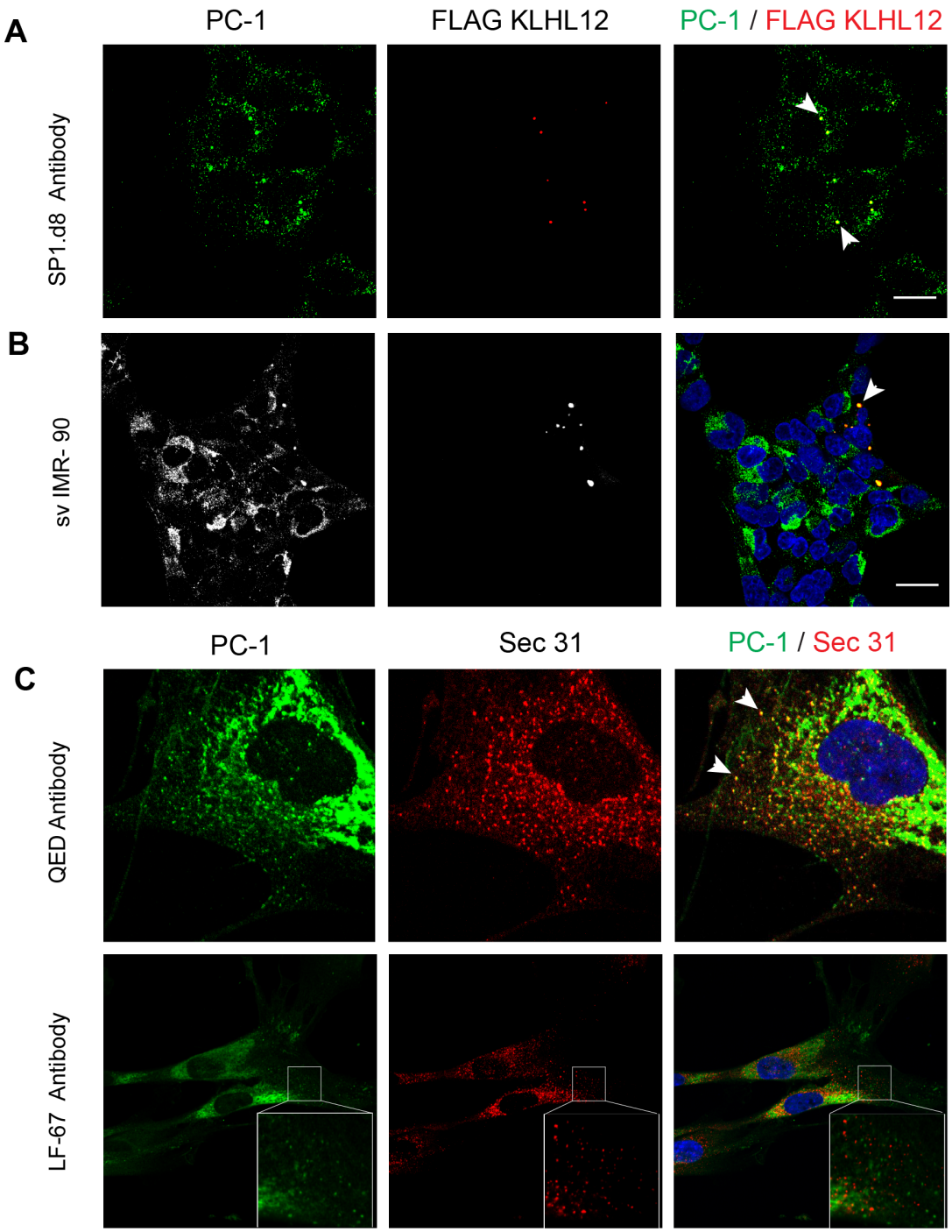

Figure 2. S2: A. KI6 cells were induced for Klhl12 expression for 7.5 hours with doxycycline and labeled with a monoclonal antibody SPI.D8 recognizing PC1. Arrows indicate puncta co-localizing for Klhl12 and PC1. **B**. svIMR90 cells were transfected with Klhl12. Double immunofluorescence using PC1 and FLAG antibodies revealed puncta that co-localized for both markers (indicated by arrow) **C.** Panel shows comparison of labeling efficiency of two PC1 antibodies – QED (monoclonal) and LF-67 (polyclonal) in IMR90 cells. Arrow indicates Sec31/PC1 co-localizing puncta

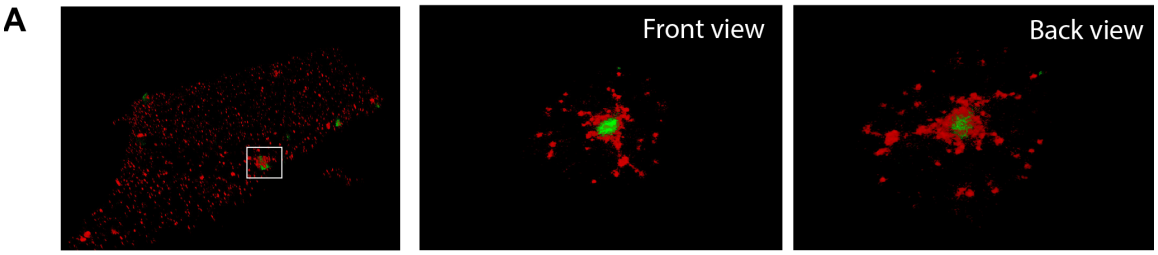

Figure 2. S2: KI6 cells were induced for Klhl12 expression for 7.5 hours with doxycycline and labeled with a antibodies recognizing PC1 and KLHL12 and imaged by Ground State Depletion (GSD) STORM. Boxed area in the overview is magnified to show PC-1 (green) inside a Sec31 (red) labeled vesicle.

Chapter 3: Ultrastructure of procollagen-1 carrying COPII vesicles

Introduction

In this chapter I will discuss the techniques I employed to arrive at the ultrastructure of the large COPII vesicles. This part of the study was designed to understand the morphology of these carriers: are they free vesicles or tubules? Our current understanding of the morphology of canonical COPII vesicles trafficking regular small cargo comes from reconstituted systems using cell free assays and intact cells. Thin-section electron microscopy of budded vesicles from a reaction using ER membranes and purified COPII components (Sar1p, Sec23/24p and Sec13/31p proteins from yeast) showed uniform 70-80 nm vesicles (Barlowe, 1994). Cryoelectron microscopy showed coated tubular extensions generated by incubating giant unilamellar vesicles with COPII proteins (Bacia et al., 2011). In Rat Basophile Leukemia (RBL) cells, serial sections of ER exit sites imaged by electron microscopy revealed ER buds emerging from the nuclear envelope (Bannykh et al., 1996). Immunolgold labeling using COPII specific protein revealed labeling at ER buds (Martinez-Menarguez et al., 1999).

Correlative light and electron microscopy (CLEM) has recently revolutionized the field of imaging. It allows the visualization of the very same organelle by fluorescence and electron microscopy (De Boer et al., 2015). Light Microscopy offers the advantage in that it can provide wide field images of whole cells, but its resolution is limited. The advantage of electron microscopy is that it can provide much higher resolution images, up to molecular dimensions, but only over specific regions of a cell at a time and not in live cells. CLEM combines the advantages of both techniques. The types of CLEM techniques employed thus far include preserving fluorescence in resin (Kukulski et al., 2011) use of quantum dots, enzyme-based probes such as horseradish-peroxidase (HRP) and using fluoronanogold as CLEM markers (Sosinsky et al., 2007). However not much effort has been made in combining 3D correlative imaging using confocal imaging and immunogold labeling. In the following section, I will discuss the technique I developed of using 0.02 % saponin as a permeabilizing agent while performing correlative fluorescence and electron microscopy.

Results

Use of 0.02 % saponin as membrane permeabilizing agent for electron microscopy

Traditionally 0.1% Triton-X is used as standard permeabilizing agent in most laboratories for immunofluorescence. However, membrane ultrastructure is poorly preserved in this detergent at that concentration. (Figure 3.1 A) Whereas the nucleus alone seems to be well preserved, the ultrastructure of the organelles of the endomembrane system is all but completely disrupted. Saponin at 0.1%, on the other

hand, resulted in improved preservation (Figure 3.1B) This concentration has also been reported in other studies (Mironov et al., 2003). The membranes appear intact but with scope for improvement. I used 0.02% saponin as a concentration that allowed optimum penetration of probes and while preserving the ultrastructure at levels superior to that seen using 0.1% saponin. I tested this using both 1.4 nm gold conjugated secondary antibody as a secondary antibody (Figure 3.1 C) and using fluoronanogold (secondary antibody conjugated with Alexa Fluor 568 and 1.4 nm gold) in Figure 3.1 D. The preservation of the entire cell is evident on 3D Focused Ion Beam Imaging (FIB SEM) on a single cell that has been permeabilized with 0.02 % saponin (Figure 3. S1)

Large COPII vesicles are hollow membranous containers

While conventional confocal microscopy images revealed co-localized diffraction-limited puncta with no discernible morphological details, we next aimed at resolving these structures and achieving a visible separation of labels using super-resolution microscopy (STORM) and conventional electron microscopy. When puncta generated at 7.5 h of doxycycline induction of Klhl12 expression in fixed cells were immunolabeled with a Sec31A antibody conjugated with Alexa-647 fluorophore and subjected to 3D STORM analysis, we observed a hollow cage-like structure (Fig. 3.2 A). Virtual sections of the structure in XY, XZ and YZ dimensions revealed a hollow compartment surrounded by a protein coat, presumably made up of the inner and outer COPII coat protein shells. Virtual sections in Z dimension of a single puncta hinted at the structure being a shell with cavity, closing up on both ends (Fig. 3.2 B). I noticed a similar morphological feature by correlative light and electron microscopy (CLEM) on puncta co-localizing for PC1 and Sec31A markers, expressed at endogenous levels in Saos-2 cells (Fig. 3.2 C). The organelles appeared to have a single membrane, decorated with what may be remnants of a protein coat. Although the cells were permeabilized with a gentle detergent (saponin) at concentrations (0.02%) well below the established protocols, some compromise in structural integrity (morphological preservation) of the organelle may be evident. The co-localized puncta appeared to be one single compartment and not a cluster of smaller vesicles with a diameter ranging from 350 nm to 1.7 nm. The puncta had morphologies that appeared spherical to polymorphic in nature.

3D correlative confocal and FIB SEM imaging on large COPII vesicles

As an alternate approach to CLEM, I combined the techniques of confocal microscopy (acquiring Z stacks in 3D) and use of FIB/SEM (3D imaging of whole cell). As a CLEM marker, I employed fluoronanogold (secondary antibody conjugated with Alexa Fluor 568 and 1.4 nm gold) followed by silver enhancement to visualize the large COPII carriers. Specifically, I labeled Sec31, the outer COPII protein as a marker to identify COPII containers with dimensions ranging from 80 nm to 1μ. 3D Z stacks were collected for a cell displaying several large COPII cages (Fig. 3.3A). The cells were processed for gold enhancement and subsequently for FIB/SEM analysis. The very same cell was correlated using the alphanumeric pattern from the grid that got transferred into the resin surface using the secondary (SE2) detector. FIB/SEM imaging through the cell of interest

revealed a well-preserved ultrastructure of membranes and organelles. (Fig. 3.3B) Careful analysis of gold-labeled organelles revealed vesicular structures that appeared spherical in morphology. An example of this observation is illustrated in Fig.3.3C.

Discussion

Correlative Light and Electron Microscopy (CLEM) has been employed recently in several studies as a tool to supplement biochemical approaches in understanding a phenomenon and to highlight the morphology of organelles (Biazik et al., 2015; Kukulski et al., 2011) I employed this technique as a way to understand the morphology of large COPII carriers carrying procollagen-1 after several failed attempts with traditional immunogold labeling techniques. In the stably transfected cell line (HT-PC KI6), large COPII structures were discernible only in ~40% of the cell population at any time-point of doxycycline induction probably due to the fact that trafficking related events are dynamic in nature and short-lived.

A deep understanding of the molecular organization of the canonical COPII coat exists in literature; however, current understanding of ER-derived carriers involved in large cargo trafficking is limited. Using correlative light electron microscopy and tomography on fibroblasts, Mironov et al. identified large saccular transport carriers (>300 nm).These carriers were uncoated but were flanked by areas showing budding profiles. The lack of an evident coat on these large carriers might be due to instability of the COPII coat . Combining immunogold labeling and electron tomography in HepG2 cells COPII-coated ER-associated buds, and dumbbell- shaped 150–200 nm long tubules that were partially coated with COPII were observed (Zeuchner et al 2006). However, no secretory cargo was analyzed in this study. Using a combination of confocal and 3D electron microscopy, I was able to visualize large hollow membranous organelles (Fig. 3.2) that were pleomorphic in nature (ranging in size from 300nm to at times 1.5µ)

While 3D electron microscopy techniques such as Serial Block Face (SBF/SEM) and FIB/SEM are now widely employed, I have made an attempt to combine the use of a 3D imaging technique post-immunogold labeling using a CLEM marker (fluoronanogold). With superior preservation using 0.02% saponin as a permeabilization agent, I was able to visualize large COPII coated vesicles (Fig. 3.3) thus confirming our model that COPII coated vesicles indeed play a role in trafficking large cargo such as procollagen-1 wherein COPII completely encapsulates the cargo and acts as a post-ER trafficking carrier.

Materials and Methods

Correlative Light and Electron Microscopy (CLEM)

Saos-2 cells were grown on gridded 35 mm glass bottom dishes (MatTek Corporation, Ashland, USA) and fixed with double strength paraformaldehyde. The cells were processed for immunofluorescence as above with the exception that 0.02% saponin was used as the permeabilizing agent. The cells displaying co-localized PC1/SEC31A spots were imaged on a Zeiss 710 Confocal Microscope using a C-Plan Apochromat 63X/1.2 W objective followed by marking the alphanumeric location using a 5X / 0.12 NA objective. A Z-stack series of the cell of interest was also collected. When fluoronanogold (1:50) was used, gold enhancement was performed at this stage according to manufacturer's instructions. (Nanoprobes) The cells were then fixed for 30min in 0.1M cacodylate buffer, pH 7.2, containing 2% glutaraldehyde, and subsequently washed with buffer prior to post-fixation with 1% osmium tetroxide on ice. This was followed by staining with 1% aqueous uranyl acetate for 30min at room temperature. For dehydration with progressive lowering of temperature, each incubation period was 10 min, with exposure to 35% ethanol at 4°C, to 50% ethanol and 70% ethanol at −20°C, and 95%, and 100% ethanol at −35°C. Cells were restored to room temperature in 100% ethanol before embedding in an Epon resin. The cell of interest was located by the grid location on the resin and thin (70-100nm) serial sections were collected on Formvar-coated 200-mesh copper grids and post-stained with 2% aqueous uranyl acetate and 2% tannic acid. The sections were imaged at 120 kV using a Tecnai 12 Transmission Electron Microscope (FEI, Eindhoven, Netherlands). Regions of interest were correlated manually by correlating the Z slices of the confocal stack with the serial sections and overlaying the fluorescent image over the TEM image by marking down prominent landmarks in the cell such as the nuclear boundary, vacuoles and mitochondria. The overlay was also confirmed using the Icy software package.

STORM imaging

Dye-labeled cell samples were mounted on glass slides with a standard STORM imaging buffer consisting of 5% (w/v) glucose, 100 mM cysteamine, 0.8 mg/ml glucose oxidase, and 40 μg/ml catalase in 1M Tris-HCL (pH 7.5). Coverslips were sealed using Cytoseal 60. STORM imaging was performed on a home-built setup based on a modified Nikon Eclipse Ti-U inverted fluorescence microscope using a Nikon CFI Plan Apo λ 100x oil immersion objective (NA 1.45). Dye molecules were photo switched to the dark state and imaged using either 647- or 560-nm lasers (MPB Communications); these lasers were passed through an acousto-optic tunable filter and introduced through an optical fiber into the back focal plane of the microscope and onto the sample at intensities of ~2 kW cm^{-2}. A translation stage was used to shift the laser beams towards the edge of the objective so that light reached the sample at incident angles slightly smaller than the critical angle of the glass-water interface. A 405-nm laser was used concurrently with either the 647- or 560-nm lasers to reactivate fluorophores into the emitting state. The

power of the 405-nm laser (typical range 0-1 W cm^{-2}) was adjusted during image acquisition so that at any given instant, only a small, optically resolvable fraction of the fluorophores in the sample was in the emitting state. Emission was recorded with an Andor iXon Ultra 897 EM-CCD camera at a framerate of 110 Hz, for a total of ~80,000 frames per image. For three-color imaging, we first performed imaging by two color channels separately and sequentially using separate emission filters and excitation lasers. A ratiometric detection scheme was employed to concurrently collect the emission of Alexa Fluor 647 and CF680 in the first color channel (Bossi et al., 2008; Testa et al., 2010). Emission of these dyes was split into two light paths using a long pass dichroic mirror (T685lpxr; Chroma), each of which were projected onto one half of an Andor iXon Ultra 897 EM-CCD camera. For dye assignment, we first localized and recorded the intensity of switching events in each channel. The 560 color channel was subsequently imaged using the reflected light path of the dichroic mirror to minimize misalignment between color channels. For 3D STORM imaging, a cylindrical lens was inserted into the imaging path so that images of single molecules were elongated in opposite directions for molecules on the proximal and distal sides of the focal plane (Huang et al., 2008). The raw STORM data was analyzed according to previously described methods (Huang et al., 2008; Rust et al., 2006).

FIB SEM Imaging

For FIB/SEM imaging, we employed a Zeiss Auriga FIB/SEM workstation (Carl Zeiss Microscopy, LLC, Thornwood, NY) equipped with a Cobra Gallium column (probe size <2 nm) and a Gemini electron column (probe size < 0.8 nm). An energy-selective in-lens high-sensitivity backscattered electron detector was used for image acquisition. Slicing was achieved by using 30 kV of focused Gallium ion beam with a probe current of 240 pA. Images were recorded after each round of ion beam milling using the SEM beam at 1.5 keV, with an energy filter bias set at 750 eV. Data acquisition occurred in an automated way using the ZEISSSMARTSEM software (Carl Zeiss Microscopy, LLC, Thornwood, NY), with an XY pixel size of 3 nm and Z-step size of 10 nm, resulting in typical volumes of 40 μm by 8 μm by 15 μm.

In Silico enchancement of gold signal

Using Adobe Photoshop, a duplicate layer of electron micrograph images was created. The threshold of this layer was set to "2," leaving only the signal of the extremely saturated gold particles. The "Minimum" filter was applied with a radius of 2 pixels to increase the size of the remaining selection. White background pixels were removed, leaving the enlarged gold particles overlayed above the original image.

Figures:

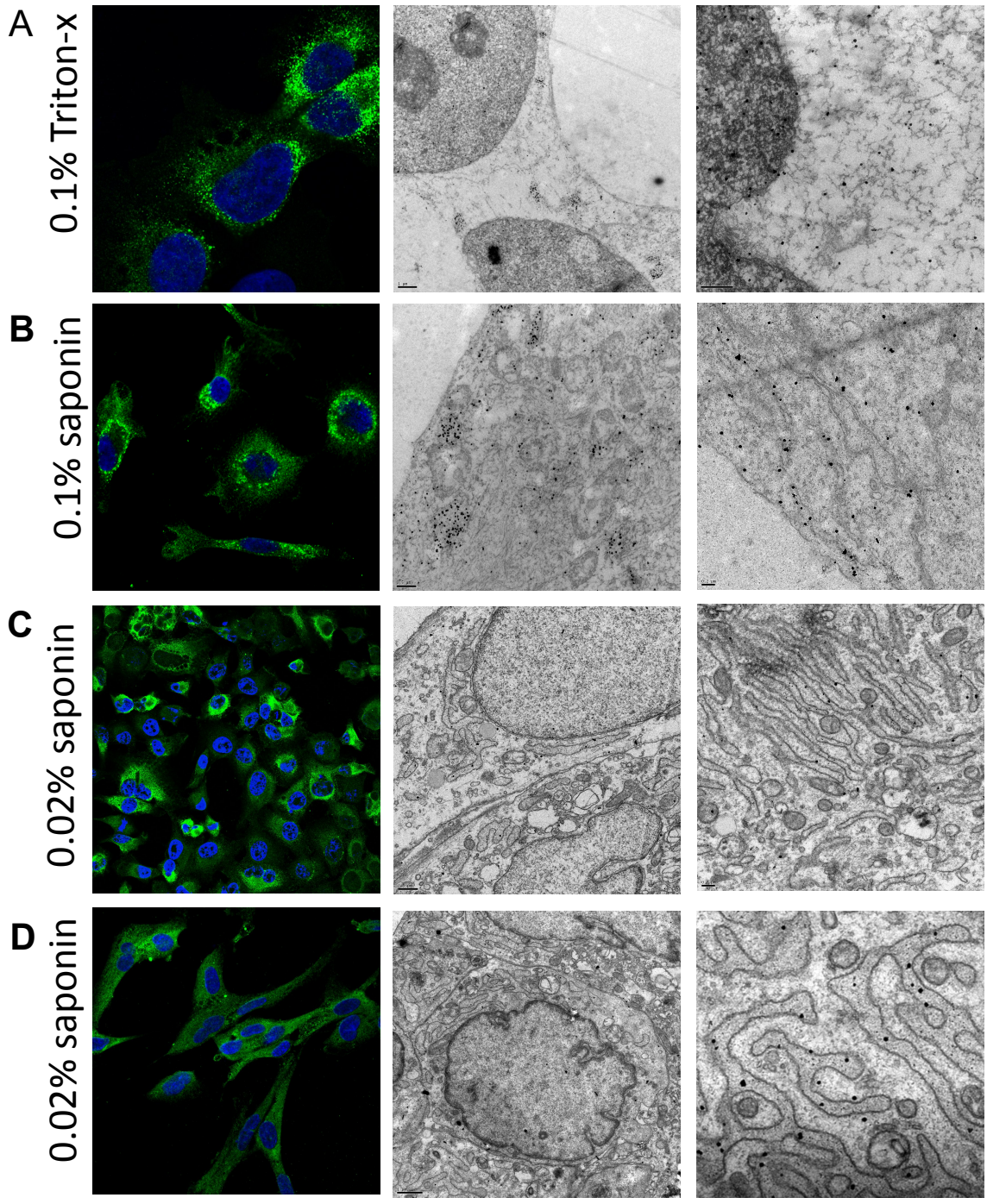

Figure 3.1: Use of 0.02% saponin as a permeabilization agent in electron microscopy

KI6 cells were permeablized using 0.1% Triton-X (**A**) or 0.1% saponin (B) or 0.02% saponin (C,D), stained for PC1 and processed for electron microscopy. Left panel shows

fluorescent images, middle panel shows images taken at 2000x magnification and the right panel shows images at a 6000x magnification. IgG conjugated with 1.4 nm gold was used a secondary antibody in B and C while fluornonanogold (Alexa fluor 568 conjugated with 1.4 nm gold) was used in D.

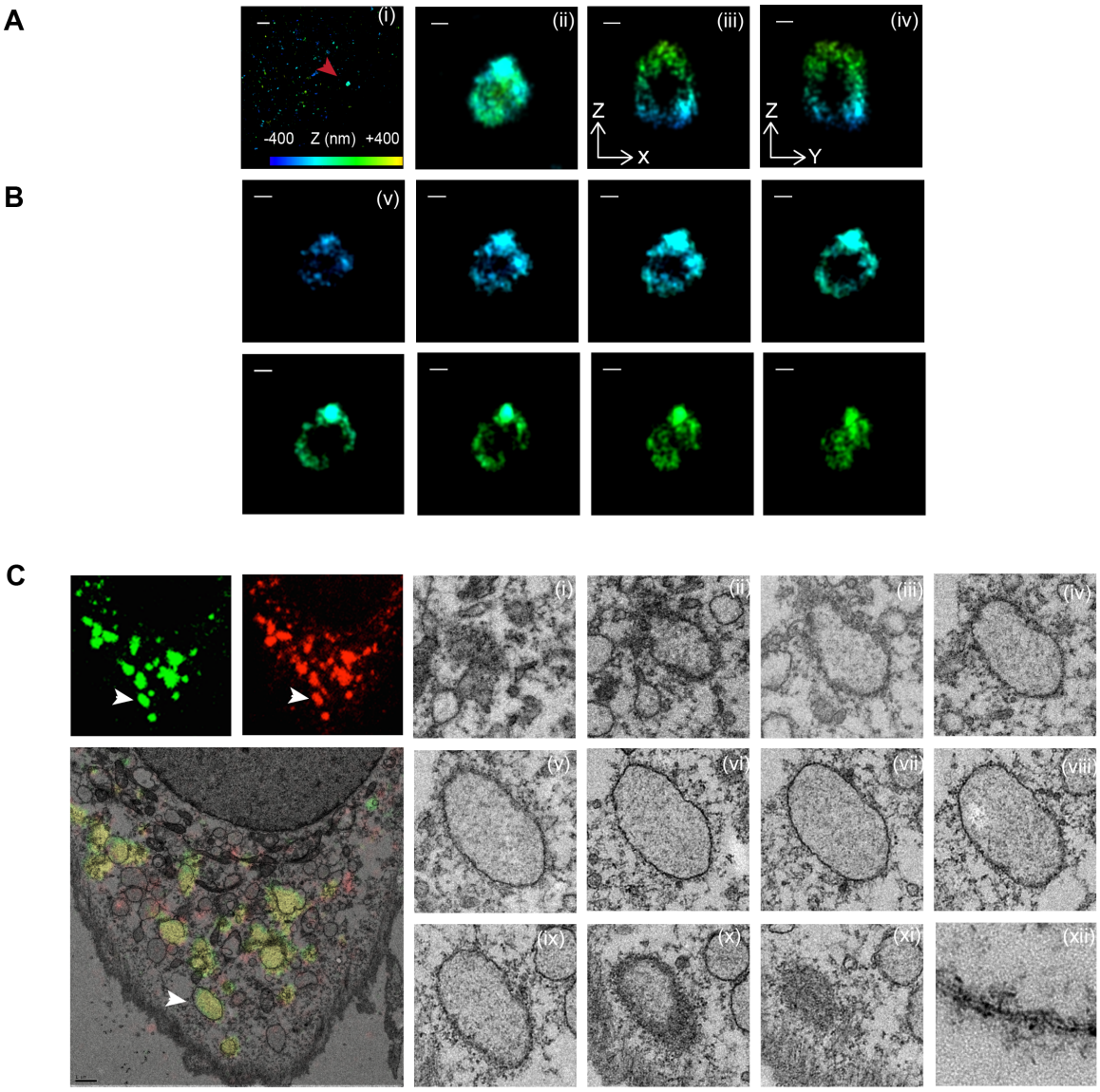

Figure 3.2: Large COPII vesicles are hollow membranous containers.
A. KI6 cells were treated with doxycycline for 7.5 hours to induce the expression of Klhl12. Single-color 3D STORM imaging was performed on immunostained Sec31A vesicles. (i) Conventional fluorescence microscopy view (ii) A XY-projection of the resulting STORM image (solid inset; bottom left) shows a 300-nm vesicle. Virtual 3D sections in XZ (iii), YZ (iv) and XY (v) reveal a hollow compartment **(B)** Scale bars: 1 µm (top); 100 nm (bottom). **C.** Saos-2 cells growing at steady state were immunostained for Sec31A (red) and PC1 (green). A representative cell showing co-localizing puncta (indicated by white arrow) was processed for CLEM. (i-xi) Serial sections of 70 nm thickness through structure of interest. (xii) Boxed area in (v) is magnified to show a lipid bilayer of the organelle.

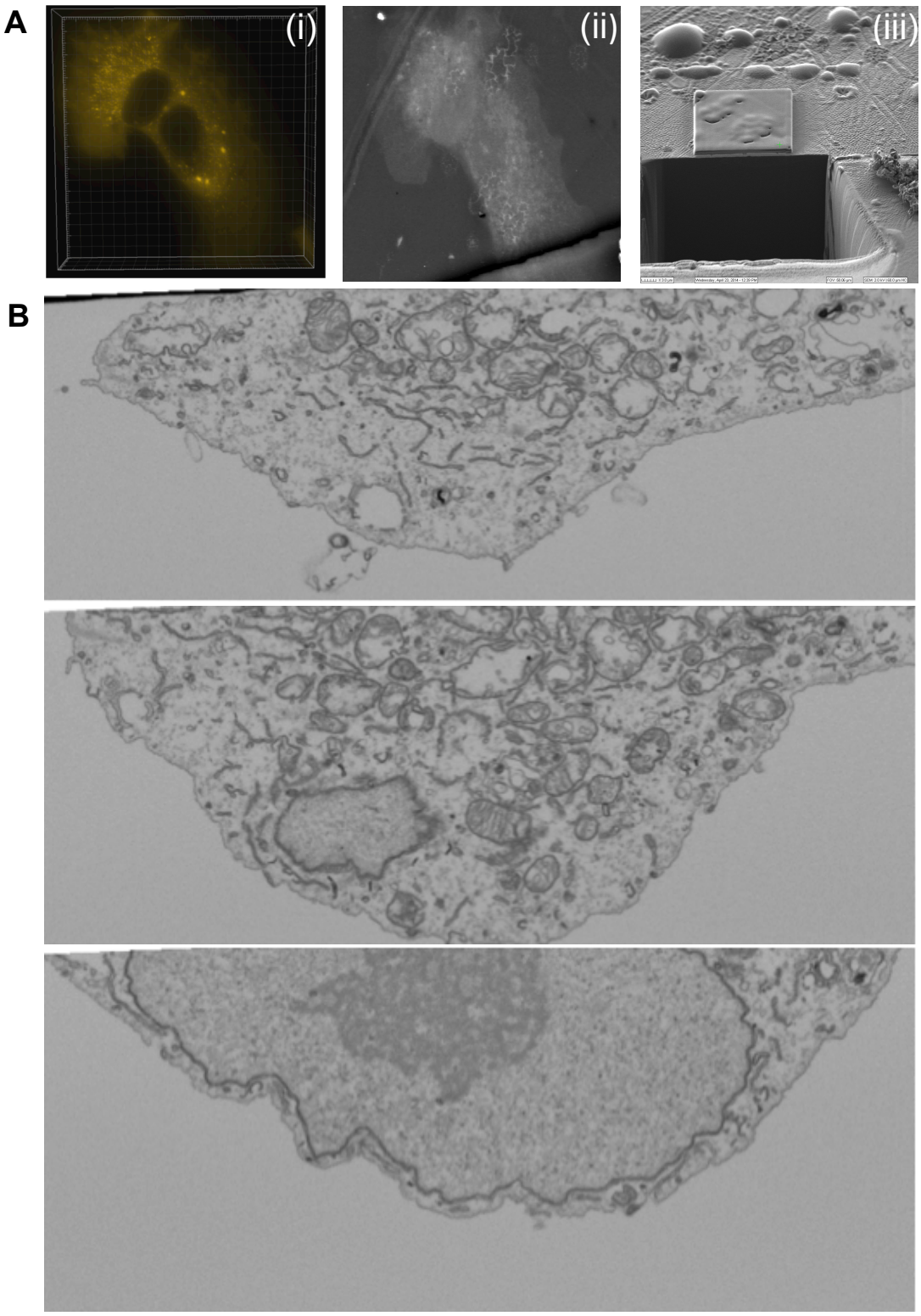
A
(i)
(ii)
(iii)
B

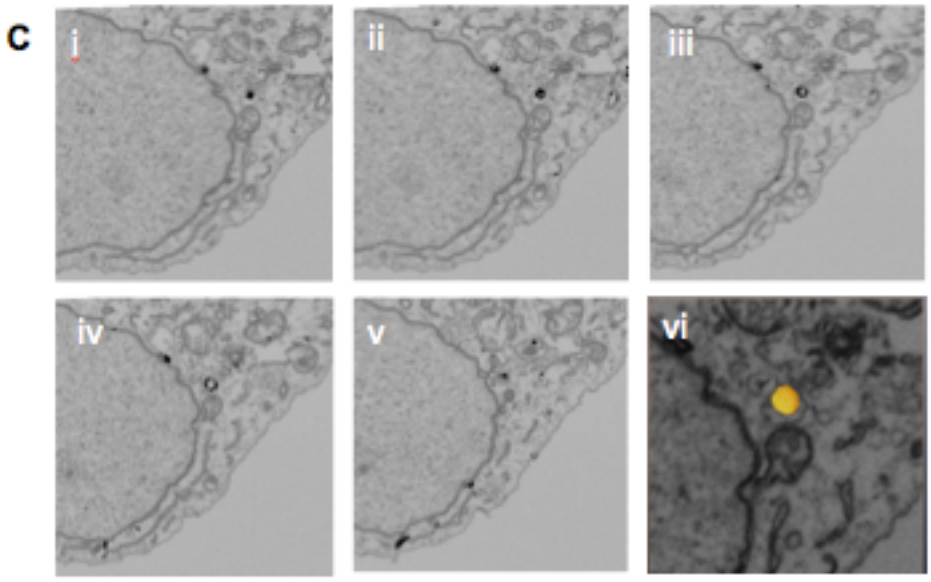

Figure 3.3: 3D correlative confocal and FIBSEM imaging

KI6 cells were induced with doxycycline for 7.5 h for KLHL12 expression. Immunofluorescence was first performed using 0.02% saponin with Sec31 antibody and fluoronanogold (CLEM) marker as a secondary antibody for simultaneous detection in light and electron microscopy modalities. **A**. (i) Cell imaged by confocal microscopy. (ii) Same cell observed on the scanning electron microscope. (iii) Trench created for FIBSEM microscopy. **B**. Representative slices (slice no. 5, slice no. 342 and slice no. 621) through the FIB stack **C.** i-v: Slices through the FIBSEM stack showing gold decorated vesicle stained for the SEC31 marker. A 3D rendering of the vesicle is shown in (vi) created using the visualization software Amira.

Supplementary Figures

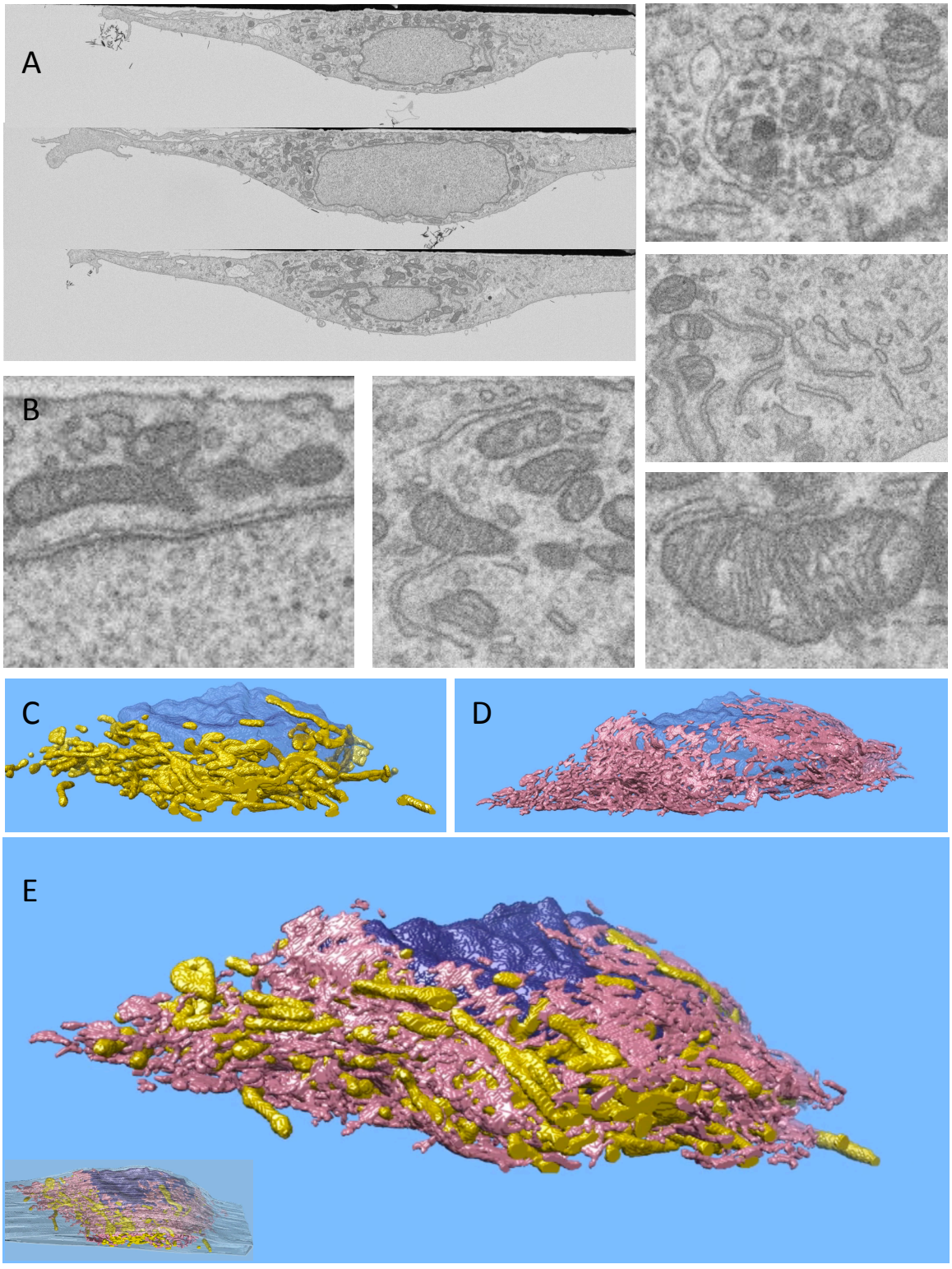
A
B
C
D
E

Figure 3.1S: FIB/SEM imaging on 0.02% saponin permeabilized cell.

KI6 cells were induced with doxycycline for 7.5 h for Klhl12 expression. Cells were processed for immunofluorescence labeling of large COPII cages by permeabilizing the cells with 0.02% saponin and processed for FIB/SEM imaging **A**. Slices through a FIB/SEM stack of a detergent permeabilized cell. **B**. 2D images from several different regions in the cell. **C**-**E** 3D rendering of the entire cell highlighting the organelles mitochondria (yellow), endoplasmic reticulum (pink) and nucleus (blue) reconstructed from the slices obtained with FIB/SEM imaging.

References

Antonny, B., P. Gounon, R. Schekman, and L. Orci. 2003. Self-assembly of minimal COPII cages. *EMBO Rep.* 4:419–24. doi:10.1038/sj.embor.embor812.

Bächinger, H.P., K.J. Doege, J.P. Petschek, L.I. Fessler, and J.H. Fessler. 1982. Structural implications from an electron microscopic comparison of procollagen V with procollagen I, pro-collagen I, procollagen IV, and a Drosophila procollagen. *J. Biol. Chem.* 257:14590–2.

Bacia, K., E. Futai, S. Prinz, A. Meister, S. Daum, D. Glatte, J.A. Briggs, and R. Schekman. 2011. Multibudded tubules formed by COPII on artificial liposomes. *Sci Rep*. 1:17. doi:10.1038/srep00017.

Bannykh, S.I., T. Rowe, and W.E. Balch. 1996. The organization of endoplasmic reticulum export complexes. *J. Cell Biol.* 135:19–35. doi:10.1083/jcb.135.1.19.

Barlowe, C., L. Orci, T. Yeung, M. Hosobuchi, S. Hamamoto, N. Salama, M.F. Rexach, M. Ravazzola, M. Amherdt, and R. Schekman. 1994. COPII: a membrane coat formed by Sec proteins that drive vesicle budding from the endoplasmic reticulum.*Cell*. 77:895–907.

Barlowe, C.K., and E.A. Miller. 2013. Secretory protein biogenesis and traffic in the early secretory pathway. *Genetics*. 193:383–410. doi:10.1534/genetics.112.142810.

Boyadjiev, S.A., J.C. Fromme, J. Ben, S.S. Chong, C. Nauta, D.J. Hur, G. Zhang, S. Hamamoto, R. Schekman, M. Ravazzola, L. Orci, and W. Eyaid. 2006. Cranio-lenticulo-sutural dysplasia is caused by a SEC23A mutation leading to abnormal endoplasmic-reticulum-to-Golgi trafficking. *Nat. Genet.* 38:1192–7. doi:10.1038/ng1876.

Bossi, M., J. lling, V.N. Belov, V.P. Boyarskiy, R. Medda, A. Egner, C. Eggeling, A. nle, and S.W. Hell. 2008. Multicolor far-field fluorescence nanoscopy through isolated detection of distinct molecular species. *Nano letters*. 8:2463–2468. doi:10.1021/nl801471d.

De Boer, P., Hoogenboom, J. P. & Giepmans, B. N. Correlated light and electron microscopy: ultrastructure lights up! *Nat. Methods* **12**, 503–13 (2015).

Fromme, J.C., and R. Schekman. 2005. COPII-coated vesicles: flexible enough for large cargo?*Curr. Opin. Cell Biol.* 17:345–52. doi:10.1016/j.ceb.2005.06.004.

Garbes, L., K. Kim, A. Rieß, H. Hoyer-Kuhn, F. Beleggia, A. Bevot, M.J. Kim, Y.H. Huh, H.-S.S. Kweon, R. Savarirayan, D. Amor, P.M. Kakadia, T. Lindig, K.O. Kagan, J. Becker, S.A. Boyadjiev, B. Wollnik, O. Semler, S.K. Bohlander, J. Kim, and C. Netzer. 2015. Mutations in SEC24D, encoding a component of the COPII machinery, cause a

syndromic form of osteogenesis imperfecta. *Am. J. Hum. Genet.* 96:432–9. doi:10.1016/j.ajhg.2015.01.002.

Ishida, Y., and K. Nagata. 2011. Hsp47 as a collagen-specific molecular chaperone. *Meth. Enzymol.* 499:167–82. doi:10.1016/B978-0-12-386471-0.00009-2.

Jensen, D., and R. Schekman. 2011. COPII-mediated vesicle formation at a glance. *J. Cell. Sci.*124:1–4. doi:10.1242/jcs.069773.

Kim, S.-D.D., K.B. Pahuja, M. Ravazzola, J. Yoon, S.A. Boyadjiev, S. Hammamoto, R. Schekman, L. Orci, and J. Kim. 2012. SEC23-SEC31 interface plays critical role for export of procollagen from the endoplasmic reticulum. *J. Biol. Chem.* 287:10134–44. doi:10.1074/jbc.M111.283382.

Kim, J., S. Hamamoto, M. Ravazzola, L. Orci, and R. Schekman. 2005. Uncoupled packaging of amyloid precursor protein and presenilin 1 into coat protein complex II vesicles. *J. Biol. Chem.* 280:7758–68. doi:10.1074/jbc.M411091200.

Kukulski, W, M Schorb, S Welsch, and A Picco. 2011. Correlated fluorescence and 3D electron microscopy with high sensitivity and spatial precision. *The Journal of cell Biology* doi:10.1083/jcb.201009037.

Jin, L., K.B. Pahuja, K.E. Wickliffe, A. Gorur, C. Baumgärtel, R. Schekman, and M. Rape. 2012. Ubiquitin-dependent regulation of COPII coat size and function. *Nature*. 482:495–500. doi:10.4161/cl.20372.

Malhotra, V., and P. Erlmann. 2015. The pathway of collagen secretion. *Annu. Rev. Cell Dev. Biol.* 31:109–24. doi:10.1146/annurev-cellbio-100913-013002.

Martínez-Menárguez, J.A., H.J. Geuze, J.W. Slot, and J. Klumperman. 1999. Vesicular tubular clusters between the ER and Golgi mediate concentration of soluble secretory proteins by exclusion from COPI-coated vesicles. *Cell*. 98:81–90. doi:10.1016/S0092-8674(00)80608-X.

Matsuoka, K., L. Orci, M. Amherdt, S.Y. Bednarek, S. Hamamoto, R. Schekman, and T. Yeung. 1998. COPII-coated vesicle formation reconstituted with purified coat proteins and chemically defined liposomes.*Cell*. 93:263–75. doi:10.1016/S0092-8674(00)81577-9.

McCaughey, J., V.J. Miller, N.L. Stevenson, A.K. Brown, A. Budnik, K.J. Heesom, D. Alibhai, and D.J. Stephens. 2016. TFG Promotes Organization of Transitional ER and Efficient Collagen Secretion. *Cell Reports*. 15:1648–1659. doi:10.1016/j.celrep.2016.04.062.

Merte, J., D. Jensen, K. Wright, S. Sarsfield, Y. Wang, R. Schekman, and D.D. Ginty. 2010. Sec24b selectively sorts Vangl2 to regulate planar cell polarity during neural tube closure. *Nat. Cell Biol.*12:41–6; sup pp 1–8. doi:10.1038/ncb2002.

Mironov, A.A., A.A. Mironov, G.V. Beznoussenko, A. Trucco, P. Lupetti, J.D. Smith, W.J. Geerts, A.J. Koster, K.N. Burger, M.E. Martone, T.J. Deerinck, M.H. Ellisman, and A. Luini. 2003. ER-to-Golgi carriers arise through direct en bloc protrusion and multistage maturation of specialized ER exit domains. *Dev. Cell*. 5:583–94. doi:10.1016/S1534-5807(03)00294-6.

Narayan, K., C.M. Danielson, K. Lagarec, B.C. Lowekamp, P. Coffman, A. Laquerre, M.W. Phaneuf, T.J. Hope, and S. Subramaniam. 2013. Multi-resolution correlative focused ion beam scanning electron microscopy: Applications to cell biology. *J. Struct. Biol.*doi:10.1016/j.jsb.2013.11.008.

Nogueira, C., P. Erlmann, J. Villeneuve, A.J.J. Santos, E. Martínez-Alonso, J.Á.Á. Martínez-Menárguez, and V. Malhotra. 2014. SLY1 and Syntaxin 18 specify a distinct pathway for procollagen VII export from the endoplasmic reticulum. *Elife*. 3:e02784. doi:10.7554/eLife.02784.

Presley, J.F., N.B. Cole, T.A. Schroer, K. Hirschberg, K.J. Zaal, and J. Lippincott-Schwartz. 1997. ER-to-Golgi transport visualized in living cells. *Nature*. 389:81–5. doi:10.1038/38001.

Saito, K., K. Yamashiro, Y. Ichikawa, P. Erlmann, K. Kontani, V. Malhotra, and T. Katada. 2011. cTAGE5 mediates collagen secretion through interaction with TANGO1 at endoplasmic reticulum exit sites.*Mol. Biol. Cell*. 22:2301–8. doi:10.1091/mbc.E11-02-0143.

Satoh, M., K. Hirayoshi, S. Yokota, N. Hosokawa, and K. Nagata. 1996. Intracellular interaction of collagen-specific stress protein HSP47 with newly synthesized procollagen. *J. Cell Biol.* 133:469–83. doi:10.1083/jcb.133.2.469.

Scales, S. J., Pepperkok, R. & Kreis, T. E. Visualization of ER-to-Golgi transport in living cells reveals a sequential mode of action for COPII and COPI. *Cell* **90**, 1137–48 (1997).

Shima, D.T., S.J. Scales, T.E. Kreis, and R. Pepperkok. 1999. Segregation of COPI-rich and anterograde-cargo-rich domains in endoplasmic-reticulum-to-Golgi transport complexes. *Curr. Biol.*9:821–4. doi:10.1016/S0960-9822(99)80365-0.

Stephens, D.J., and R. Pepperkok. 2002. Imaging of procollagen transport reveals COPI-dependent cargo sorting during ER-to-Golgi transport in mammalian cells. *J. Cell. Sci.* 115:1149–60.

Testa, I, CA Wurm, R Medda, and E Rothermel. 2010. Multicolor fluorescence nanoscopy in fixed and living cells by exciting conventional fluorophores with a single wavelength. *Biophysical journal*. doi:10.1016/j.bpj.2010.08.012.

Townley, A.K., Y. Feng, K. Schmidt, D.A. Carter, R. Porter, P. Verkade, and D.J. Stephens. 2008. September 1. "Efficient coupling of Sec23-Sec24 to Sec13-Sec31 drives

COPII-dependent collagen secretion and is essential for normal craniofacial development." *Journal of cell science* 121 Pt 18 (September 1): 3025–34. doi:10.1242/jcs.031070. http://www.ncbi.nlm.nih.gov/pubmed/18713835.

Venditti, R., T. Scanu, M. Santoro, G. Tullio, A. Spaar, R. Gaibisso, G.V. Beznoussenko, A.A. Mironov, A. Mironov, and L. Zelante. 2012. Sedlin controls the ER export of procollagen by regulating the Sar1 cycle. *Science*. 337:1668–1672.

Wilson, D.G., K. Phamluong, L. Li, M. Sun, T.C. Cao, P.S. Liu, Z. Modrusan, W.N. Sandoval, L. Rangell, R.A. Carano, A.S. Peterson, and M.J. Solloway. 2011. Global defects in collagen secretion in a Mia3/TANGO1 knockout mouse. *J. Cell Biol.*193:935–51. doi:10.1083/jcb.201007162.

Zanetti, G., K.B. Pahuja, S. Studer, S. Shim, and R. Schekman. 2012. COPII and the regulation of protein sorting in mammals. *Nat. Cell Biol.* 14:20–8. doi:10.1038/ncb2390.